Fall 12-1-2018

Hydrogen Bond Mediated Water Structuring, Diffusion, and Elastic Properties in Acrylamide Copolymer Glycohydrogels

April Levu Fogel
University of Southern Mississippi

HYDROGEN BOND MEDIATED WATER STRUCTURING, DIFFUSION, AND ELASTIC PROPERTIES IN ACRYLAMIDE COPOLYMER GLYCOHYDROGELS

by

April L. Fogel

A Dissertation
Submitted to the Graduate School,
the College of Arts and Sciences
and the School of Polymer Science and Engineering
at The University of Southern Mississippi
in Partial Fulfillment of the Requirements
for the Degree of Doctor of Philosophy

Approved by:

Dr. Sarah E. Morgan, Committee Chair
Dr. Sergei I. Nazarenko
Dr. Robert Y. Lochhead
Dr. James W. Rawlins
Dr. Gopinath Subramanian

Dr. Sarah E. Morgan Committee Chair	Dr. Jeffrey Wiggins Director of School	Dr. Karen S. Coats Dean of the Graduate School

December 2018

ABSTRACT

Glycohydrogels have recently gained considerable interest as biocompatible and high water content hydrogels that have similar physicochemical nature to the cell membrane, making them ideal materials for targeted biomedical and personal care applications (e.g., drug delivery systems, biosensors, and contact lenses). Regardless of the specific application, water-polymer and water-water hydrogen bonding interactions have been shown to dictate hydration stability and diffusional properties in traditional hydrogel architectures (e.g., crosslinked HEMA). However, due to the development of glycohydrogel materials within the past two decades, most literature focuses on synthetic techniques and general hydration characteristics. Furthermore, scant literature examines the effect of hydrophobically modified glycohydrogels on hydrogen bonding modes and diffusion characteristics.

This dissertation explores the fundamental physicochemical nature of hydrophobically modified glycohydrogels containing pendant galactose and siloxane moieties. An experimental and simulation approach was utilized to examine the effect of amphipathic balance and crosslink density on bound water content, water mobility, and desorption kinetics for hydrophobically modified glycohydrogels swollen in water. We found that bound water can be tuned in high water content glycohydrogels with the addition of hydrophobic comonomers. Finally, the sol/gel transition kinetics and development of network modulus was monitored via UV-rheology for a series of homopolymer and copolymer glycohydrogels containing systematically varied crosslinker and hydrophobic comonomer loadings. The viscoelastic properties of the as-prepared hydrogels as a function of frequency were used to reveal characteristic features

(e.g., loss and storage modulus) associated with the type of network architecture developed. Homopolymer glycohydrogels exhibited viscoelastic behavior suggestive of the formation of hydrogen-bonded clusters among pendant saccharide groups. Addition of hydrophobic comonomers aided in the dissociation of these clusters but also significantly reduced the elastic modulus of the glycohydrogel network.

ACKNOWLEDGMENTS

It has been a long, arduous journey that has challenged me intellectually, emotionally, and at times physically; changing the face of who I am both professionally and personally. I remain humbled by the hardships that I endured and will be forever grateful for all the help and guidance I received from many exceptional people along the way. Amongst them, I would like to acknowledge…

… My advisor, Dr. Sarah E. Morgan for believing in me even when I did not believe in myself. Thank you for your unwavering and whole-hearted support, patients, and mentorship throughout my scientific and professional development.

…Dr. Lisa Kemp, without your help during the final hours I would not have finished, and for that, I will be forever grateful. Thank you for your candid words of wisdom and scientific insight.

… My committee members, Dr. Sergie Nazarenko, Dr. Robert Locchead, Dr. James Rawlins, and Dr. Gopinath Subramanian, for your guidance during my education.

…My collaborators at Texas Technical University, Ashwin, Mani, and Dr. Khare, for the hours of discussion and rewrites. Working with you exposed me to the world of molecular dynamic simulations, providing me with a crash course education in MDS and valuable experience of the challenges associated with communication across disciplines.

…Dr. Levi Moore for teaching me chemistry and all the laboratory techniques associated with doing chemistry. You have been such an integral piece to my scientific development and a phenomenal friend who I could lean on during those difficult times.

…My colleagues in the Morgan Research Group (MRG) Thank you, Dr. Katrina Knauer, Dr. Qi Wu, Dr. Sarah Exley, Ashleigh Bristol, Pradipta Das, Kelli Stockmal, and Mitchel Woellner, for all the laughter, late nights in the lab, and shenanigans.

…Bishal Upadayah thank you for always working so hard. It has been a pleasure to be your mentor, I wish you all the best in your future career endeavors and never hesitate to reach out to me for anything.

…My sisters: Anna Fogel for exposing me to the magic of 80's music. I am so lucky to have you as my best friend and role model. Healani Sonoda-Pale for laying my educational foundation during my childhood years in Hilo and instilling in me a sense of cultural identity that stems from your tenacious advocacy for the rights of indigenous peoples. Leihinahina Sullivan for being the most irritating of the three loca's who taught me how to have fun, be loud, and unapologetic for who I am.

…My niece and nephews: Kea Sullivan, Punia Pale, Ulu Puhi Pale, and Kapono Sullivan, for your love and support.

…My home girls: Laila Moire-Selvage, Martha Duer, and Erin Chung, for always making me laugh and keeping me grounded. You ladies make life fun, and I am proud of all of you.

…Madeline Commander, for being the most supportive and understanding best friend and companion during these months of writing. I hope I can be there for you during these next stages in your career and I look forward to what life has in store for us.

…Finally numerous other faculty, staff, and colleagues for their Kimberly Wingo, Dana, Meleanie Heuser, Mrs. Vicky; Dr. William Jarret, Dr. Jeffery Wiggons, Morgan Heskett, and Ryan Dufree

DEDICATION

This dissertation is dedicated to my mother, Lorraine Sonoda-Fogel, M.D and father, Frederick Fogel.

Thank you for your love, support, and strength without which I could not have completed this dissertation.

TABLE OF CONTENTS

LIST OF TABLES

LIST OF ILLUSTRATIONS

CHAPTER I – Research Background

1.1 Introduction

Hydrogels are super-absorbent, three-dimensional polymer networks that absorb many times their weight in water but remain insoluble because of crosslinks. Absorptivity is defined by the total weight of water uptake in the polymeric networks, and water binding is associated with how strongly the absorbed water interacts with the hydrogel network. Hydrogels are often used in biomedical applications such as wound dressings, drug delivery, scaffolding for tissue engineering[1, 2], transport membranes, and films for ophthalmic applications,[3] where water uptake and maintenance are imperative. Research in hydrogel technologies has grown substantially, with over 70k articles published since the seminal work in the 1960's by Wichterle and Lim.[4, 5] In that work, crosslinked poly(hydroxyethyl methacrylate) (pHEMA) was reported as a hydrophilic, transparent, and mechanically robust polymeric material that exhibits no adverse immune responses when implanted into living organisms.[5] HEMA hydrogels revolutionized the contact lens (CL) industry, and since then developments in hydrogel technologies have expanded beyond simple network architectures and composition. Most notably for the CL industry was the introduction of polysiloxanes in the 1970's to mitigate oxygen permeation issues related to methacrylate networks. However, due to inherent hydrophobicity, these polymers promote protein deposition[6] and tear film disruption[7] which deteriorates the CL performance and provides adverse health implications.

Hyaluronic acid (HA), a polysaccharide found in cartilage and the vitreous humor of the eye that serves as a natural lubricating agent in the human body, displays high water absorptivity and is the subject of intense research for use in CL[6, 8, 9] and other biomedical

applications[10]. HA is an anionic, non-sulfonated glycosaminoglycan comprised of D-glucuronic acid and D-N-acetyl glucosamine (Figure 1.1). HA can be obtained from animal sources, such as rooster combs, and can be expressed in Bacillus subtilis,[11] sources which are associated with concerns related to human biocompatibility and cost. The low modulus of native HA (970 Pa)[10] networks have limited their use in CL formulations. Currently, HA is either incorporated into CL formulations through surface treatments or synthesis of interpenetrating networks (IPN). There is interest in the development of synthetic materials that mimic HA properties but have controllable structures, e.g., glycopolymers, which are synthetic analogs of naturally occurring polysaccharides, to provide a source of tailorable, readily available materials for biomedical applications.

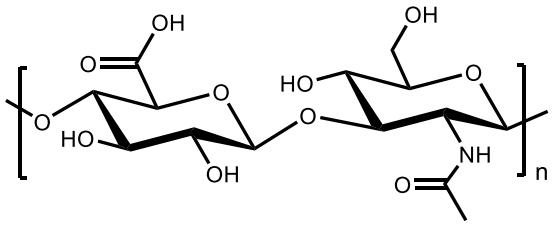

Figure 1.1 Structure of hyaluronic acid, a disaccharide comprised of D-glucuronic acid and D-N-acetyl glucosamine

In general, the basic properties required for hydrogels used in biomedical and personal care applications such as CLs include optical transparency, oxygen permeability, surface wettability, mechanical stability, and biocompatibility. Use of novel components with favorable interfacial properties (e.g., saccharide containing monomers and crosslinkers) have advanced material function, allowing for the design of hydrogels that can be used for targeted drug delivery vesicles and sensing applications. Water within the hydrogel network plays a pivotal role in determining each of these properties; however, the

precise roles of water content and water structure are not well understood.[12-15] Furthermore, there is a lack of understanding of the relationships between network architecture and water structure. Therefore, the objective of this research is to systematically investigate water absorption and structure in hydrogel networks as a function of network structure, with a specific focus on glycopolymers, to elucidate the role of water on the performance of hydrogels inspired by naturally occurring materials.

1.2 Characteristics of water within hydrogels

It has been well established that diffusional processes of solutes and polymer-water interfacial interactions within various hydrogel architectures play a pivotal role in dictating network properties and application efficiency.[16] Specifically, equilibrium water content (EWC), water structure, and water retention are crucial in dictating hydrogel function and properties in most biomedical applications.[17, 18] The EWC is a measure of the total water imbibed by the hydrogel at full saturation and is affected by the solvent environment and hydrogel network architecture such as crosslink density, functional group identity, and polymer backbone flexibility.

Bulk water is classified into three categories (free, restricted, and bound) dictated by the modes of hydrogen bonding within the polymer network, illustrated in Figure 1.2. Water confined within a polymer matrix have observable differences in thermodynamic behavior related to the degree of polymer-water hydrogen bonding modes. Free water is unassociated with hydrogen bonding sites and therefore exhibits a melting transition similar to that of pure water. Restricted water is weakly associated with the polymer network with limited hydrogen bonding, and bound water is strongly associated and undergoes multiple modes of hydrogen bonding. From an experimental perspective,

capturing interfacial water-polymer and water-water interactions is complicated because of the short time scale associated with water fluctuations (the self-diffusion coefficient of pure water is 2.29 x 10^{-9} m^2s^{-1} at 25 ºC[19, 20]). Inherent fluctuations of water are affected by both thermodynamic and kinetic factors associated with the hydration environment.

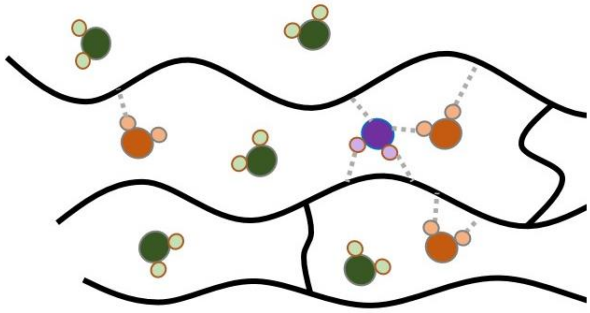

Figure 1.2 Illustration of structural water within a covalently crosslinked hydrogel network representing free (green), restricted (orange), and bound (purple) water.

Conventional methods used to identify and quantify the types of water within hydrogel networks include differential scanning calorimetry (DSC), thermogravimetric analysis (TGA), confocal Raman spectroscopy, and pulse field gradient nuclear magnetic resonance (PFG NMR) spectroscopy. The relative strength of the water-polymer interaction can be captured by the endothermic peak(s) in DSC. Dual endothermic peaks near 0 ºC and -10 ºC represent free water and restricted water respectively.[21-23] Bound water is considered non-freezable because the enthalpic transition occurs below -93 ºC and therefore is not captured by DSC.[22] Bound water is calculated using the total water content and relative amounts of free and restricted water determined by DSC. Techniques such as ^{1}H-NMR and DSC are commonly used for determining bound water composition[24] and have been found to be in good agreement.[25]

1.3 Glycohydrogels: Synthetic analogs of naturally occurring polysaccharides

Hydrogels consisting of natural polymers, or biopolymers, have been used in biomedical applications due to their biocompatibility, water absorptivity, and ease of chemical modification. Polysaccharide-based hydrogels are one such example of natural polymers that can contain more than 90% of their weight in water when swollen. Pasqui et al. examined the use of HA, chitosan (CHT), and carboxymethyl cellulose (CMC) as injectable hydrogels due to their thixotropic behavior.[10] HA was crosslinked through the carboxylate functionality using a difunctional primary amine crosslinker and Fourier-Transform Infrared Spectroscopy (FT-IR) was used to monitor the role of water and its interfacial behavior with the dry and swollen hydrogels. Kim et al. determined the amount of bound water and associated drying kinetics of interpenetrating hydrogels comprised of HA and poly(vinyl alcohol) (PA).[21] They reported that total water and free water content increased with increasing HA content. A review by M. Rah examined the use of HA in ophthalmic applications, where the incorporation of HA into contact lenses enhanced tear film formation and provided surface lubrication.[26] While polysaccharides have made significant strides in the medical field as high water content natural polymers, incorporation of these natural polymers into synthetic hydrogel networks is limited to interpenetrating network (IPN) architectures[27, 28] and surface treatments.[9]

Glycohydrogels are a unique class of superabsorbent polymer networks that contain mono, di, or tri-saccharide moieties in either the main chain, pendant group, or crosslinker (illustrated in Figure 1.3). They are synthesized using glycomonomers which are analogs of naturally occurring polysaccharides or glycans. Glycomonomers and advancements in synthetic techniques have afforded the unique ability to precisely design glycohydrogel properties through saccharide composition and organization within the

network. As a result, glycohydrogels have gained considerable interest as important biocompatible polymeric materials because of their relevance in medical applications,[29], e.g., drug delivery systems,[30, 31] tissue scaffolds,[32, 33] and biosensors.[34, 35]

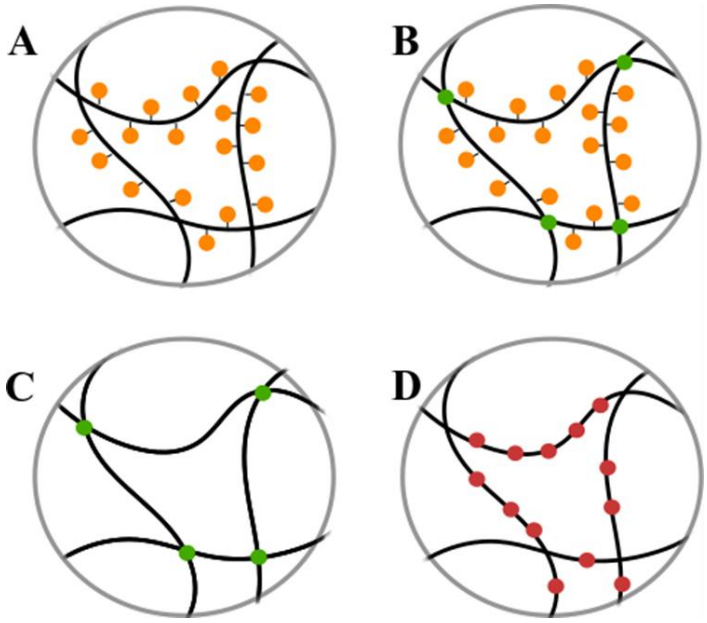

Figure 1.3 Schematic of glycohydrogel structures where the saccharide moiety is in the (A) pendant group, (B) pendant group and crosslinker, (C) crosslinker, and (D) main chain, Adapted from Burek et al.[29]

While advantageous protein/polymer interactions and cell recognition afforded by pendant saccharide groups (or moieties) provide unique glycotargeting and cell adhesive ability, the swelling properties of these glycohydrogels can contribute to application efficacy because of the vital role water plays at the material-body interface.[36] Historically, hydrophilic monomers, such as *N*-vinyl pyrrolidone (NVP), (meth)acrylate derivatives, and (meth)acrylamide derivatives, have been studied through both experimental and modeling approaches in an attempt to understand how water mobility and organization are affected by chemical composition, network architecture, and

swelling environment.[37-39] In high water content, glycohydrogel structures little has been done to determine the relationship between structural water and diffusional processes. The inherent hydrophilicity of saccharide analogs provides a unique opportunity to elucidate the relationship between hydrogen bonding propensity and diffusional processes of molecular water in highly crosslinked and high-water content hydrogels.

1.4 Hydrogel Network Morphology and Design

Hydrogel networks are generically categorized by the type of crosslink junction, e.g., covalent, ionic, and physical. Networks consisting of covalent linkages differ significantly from those containing ionic and physical crosslinks due to the irreversibility and stability of the covalent linkage. A detailed discussion of the variety of hydrogel architectures, modes of preparation, and applications are found in a book chapter by Gulrez and Al-Assaf.[40] Design parameters for covalently crosslinked networks, such as the ratio of crosslinker to monomerl[41, 42] polymer functionality,[37] monomer concentration,[43] crosslinker type,[44] and reactivity of monomer and crosslinker[45] determines the network architecture, including mesh size,[41] crosslink density, and network homogeneity. The architecture, in turn, influences network properties, including water absorption, swellability, and water structure. While, in general, the pore size and network homogeneity decrease with increasing crosslinker to monomer ratio, these factors are influenced by the kinetics of the reaction, the solvent, and the degree of water association in the reactants during the process of forming the hydrogel.[46-48] Therefore, it is essential to evaluate the reaction kinetics for our proposed glycopolymer hydrogels and determine the relationships between reaction processes, network morphology, water content, and water structure.

1.5 Motivation and Goal of Research

Glycohydrogels are a relatively new class of hydrogel materials that have significant implications for the advancement of biomedical technologies and therapeutics. Many of these applications require suitable solute diffusion and favorable interfacial interactions at the polymer surface. Previous studies have shown that water content can significantly impact the properties of hydrogel networks. Furthermore, water confined within the network exhibits different properties than bulk water. A fundamental understanding of the influence of network architecture on water structuring and rates of desorption will enable better design of glycohydrogels. Further insight into the role of structural water in hydrogel systems will be provided through comparison of the performance of high water content glycopolymer networks to reference high water content systems that contain different free to bound water ratios (low and high).

1.6 Project Objectives

1. The first objective was to characterize the degree of hydrophobic inclusion of linear acrylamide copolymers containing either N,N' dimethyl acrylamide (DMA) or 2′-acrylamidoethyl-β-D-galactopyranoside (GalEAm).
2. The second objective was to synthesize a series of hydrogels with varying amphipathic balance and crosslink density, then characterize these hydrogels for EWC, structural water distribution, and dehydration characteristics.
3. The third objective was to determine the effect of crosslink density and amphipathic balance in on the rheological properties of homopolymer and copolymer glycohydrogels. Specifically, the polymerization kinetics were measured by monitoring the sol/gel behavior using in-situ rheology, and, finally,

the as-prepared hydrogel modulus was analyzed for information about the network architecture.

1.7 References

1. Van Vlierberghe, S., et al., Toward modulating the architecture of hydrogel scaffolds: curtains versus channels. *Journal of materials science. Materials in medicine* **2008,** *19* (4), 1459-66.
2. Jonker, A. M., et al., Peptide- and Protein-Based Hydrogels. *Chemistry of Materials* **2012,** *24* (5), 759-773.
3. Nicolson, P. C. V., J., Soft contact lens polymers: an evolution. *Biomaterials* **2001,** *22*, 3273-3283.
4. Buwalda, S. J., et al., Hydrogels in a historical perspective: From simple networks to smart materials. *Journal of Controlled Release* **2014,** *190*, 254-273.
5. Wichterle, O.; LÍM, D., Hydrophilic Gels for Biological Use. *Nature* **1960,** *185*, 117.
6. Weeks, A., et al., The effects of hyaluronic acid incorporated as a wetting agent on lysozyme denaturation in model contact lens materials. *Journal of biomaterials applications* **2013,** *28* (3), 323-33.
7. Stapleton, F., et al., Silicone Hydrogel Contact Lenses and the Ocular Surface. *The Ocular Surface* **2006,** *4* (1), 24-43.
8. Scheuer, C. A., et al., Retention of conditioning agent hyaluronan on hydrogel contact lenses. *Contact lens & anterior eye : the journal of the British Contact Lens Association* **2010,** *33 Suppl 1*, S2-6.
9. Singh, A., et al., A hyaluronic acid-binding contact lens with enhanced water retention. *Contact lens & anterior eye : the journal of the British Contact Lens Association* **2014**.
10. Pasqui, D., et al., Polysaccharide-Based Hydrogels: The Key Role of Water in Affecting Mechanical Properties. *Polymers* **2012,** *4* (4), 1517-1534.
11. Frischknecht, A. L.; Curro, J. G., Improved United Atom Force Field for Poly(dimethylsiloxane). *Macromolecules* **2003,** *36* (6), 2122-2129.
12. Pafiti, K., et al., Composite hydrogels of polyacrylamide and crosslinked pH-responsive micrometer-sized hollow particles. *Soft Matter* **2016,** *12* (4), 1116-1126.
13. McConville, P. P., J., A comparison of water binding and mobility in contact lens hydrogels from NMR measurements of the water self-diffusion coefficient. *Polymer* **2000,** *41*, 9081-9088.
14. Ramamoorthy, P., et al., Contact lens material characteristics associated with hydrogel lens dehydration. (1475-1313 (Electronic)).
15. Sindt, C. W.; Longmuir, R. A., Contact Lens Strategies for the Patient with Dry Eye. *The Ocular Surface* **2007,** *5* (4), 294-307.
16. Jhon Mu, S.; Andrade, J. D., Water and hydrogels. *Journal of Biomedical Materials Research* **1973,** *7* (6), 509-522.
17. McConville, P.; Pope, J. M., Diffusion limited evaporation rates in hydrogel contact lenses. *CLAO J* **2001,** *27* (4), 186-91.

18. Chaterji, S., et al., Smart Polymeric Gels: Redefining the Limits of Biomedical Devices. *Progress in polymer science* **2007,** *32* (8-9), 1083-1122.
19. Holz, M., et al., Temperature-dependent self-diffusion coefficients of water and six selected molecular liquids for calibration in accurate 1H NMR PFG measurements. *Physical Chemistry Chemical Physics* **2000,** *2* (20), 4740-4742.
20. Mills, R., Self-diffusion in normal and heavy water in the range 1-45.deg. *The Journal of Physical Chemistry* **1973,** *77* (5), 685-688.
21. Kim, S. J. L., C. K.; Kim, S. I., Characterization of the Water State of Hyaluronic Acid and PVA IPN. *J. Appl. Poly. Sci.* **2003,** *92*, 1467-1472.
22. Tranoudis, I.; Efron, N., Water properties of soft contact lens materials. *Contact lens & anterior eye : the journal of the British Contact Lens Association* **2004,** *27* (4), 193-208.
23. Yamazaki, Y., et al., Analysis and evaluation of the ionic interaction of the novel soft contact lenses using the zwitterionic polymer gel. *Journal of Applied Polymer Science* **2009,** *114* (5), 2764-2768.
24. Gun'ko, M. V., et al., Properties of Water Bound in Hydrogels. *Gels* **2017,** *3* (4).
25. McConville, P.; Pope, J. M., A comparison of water binding and mobility in contact lens hydrogels from NMR measurements of the water self-diffusion coefficient. *Polymer* **2000,** *41* (26), 9081-9088.
26. Rah, M. J., A review of hyaluronan and its ophthalmic applications. *Optometry* **2011,** *82* (1), 38-43.
27. Hu, H. B., C. R.; Nguyen, T.; Tran, H.; Rossberg, F. US 7,279,507 B2, Oct 9, 2007.
28. Giusti, P. L., C. Biomaterial comprising hyaluronic acid and derivatives thereof in interpenetrating polymer netWorks (IPN). US 5,644,049, Jul 1997.
29. Burek, M.; Wandzik, I., Synthetic Hydrogels with Covalently Incorporated Saccharides Studied for Biomedical Applications – 15 Year Overview. *Polymer Reviews* **2018**, 1-50.
30. Kim, B.; Peppas, N. A., Synthesis and characterization of pH-sensitive glycopolymers for oral drug delivery systems. *Journal of Biomaterials Science, Polymer Edition* **2002,** *13* (11), 1271-1281.
31. Zakhireh, S., et al., Investigation of pH-sensitive galactopyranoside glycol hydrogels as effective vehicles for oral drug delivery. *Journal of Polymer Research* **2014,** *21* (4), 398.
32. Liao, S. W., et al., De Novo Design of Saccharide−Peptide Hydrogels as Synthetic Scaffolds for Tailored Cell Responses. *Journal of the American Chemical Society* **2009,** *131* (48), 17638-17646.
33. Wu, Y., et al., Galactosylated reversible hydrogels as scaffold for HepG2 spheroid generation. *Acta Biomaterialia* **2014,** *10* (5), 1965-1974.
34. Cai, Z., et al., Responsive Photonic Crystal Carbohydrate Hydrogel Sensor Materials for Selective and Sensitive Lectin Protein Detection. *ACS Sensors* **2017,** *2* (10), 1474-1481.
35. Charles, P. T., et al., A galactose polyacrylate-based hydrogel scaffold for the detection of cholera toxin and staphylococcal enterotoxin B in a sandwich immunoassay format. *Analytica Chimica Acta* **2006,** *578* (1), 2-10.

36. Bag, M. A.; Valenzuela, L. M., Impact of the Hydration States of Polymers on Their Hemocompatibility for Medical Applications: A Review. *International Journal of Molecular Sciences* **2017,** *18* (8), 1422.
37. Sekine, Y., et al., Dependence of structure of polymer side chain on water structure in hydrogels. *Polymer* **2014,** *55* (24), 6320-6324.
38. Sun, D.; Zhou, J., Effect of water content on microstructures and oxygen permeation in PSiMA–IPN–PMPC hydrogel: a molecular simulation study. *Chemical Engineering Science* **2012,** *78*, 236-245.
39. Mani, S., et al., Structure and Hydrogen Bonding of Water in Polyacrylate Gels: Effects of Polymer Hydrophilicity and Water Concentration. *The Journal of Physical Chemistry B* **2015,** *119* (49), 15381-15393.
40. Gulrez, S. K. S., A.; Phillips, G., *Syed K. H. Gulrez, Saphwan Al-Assaf and Glyn O Phillips (2011). Hydrogels: Methods of Preparation, Characterisation and Applications, Progress in Molecular and Environmental Bioengineering - From Analysis and Modeling to Technology Applications*. 2011.
41. Ikeda-Fukazawa, T., et al., Effects of crosslinker density on the polymer network structure in poly-N,N-dimethylacrylamide hydrogels. *Journal of Polymer Science Part B: Polymer Physics* **2013,** *51* (13), 1017-1027.
42. Kurecic, M. S., M.; Stana, K., UV POLYMERIZATION OF POLY (N-ISOPROPYLACRYLAMIDE) HYDROGEL. *Materials and technology* **2011,** *46*, 87-91.
43. Gundogan, N., et al., Swelling, Elasticity and Spatial Inhomogeneity of Poly(N,N-dimethylacrylamide) Hydrogels Formed at Various Polymer Concentrations. *Macromolecular Chemistry and Physics* **2004,** *205* (6), 814-823.
44. Kabiri, K., et al., Synthesis of fast-swelling superabsorbent hydrogels: effect of crosslinker type and concentration on porosity and absorption rate. *European Polymer Journal* **2003,** *39* (7), 1341-1348.
45. Lai, Y., A Novel Crosslinker for UV Copolymerization of N-vinyl Pyrrolidone and Methacrylates To Give Hydrogels. **1996**.
46. Ahmad, M. B. H., M. B., DSC studies on states of water in crosslinked PMA_co_NVP Hydrogels. *Polymer International* **1994,** *33*, 273-277.
47. Andrzejewska, E., Photopolymerization kinetics of multifunctional monomers. *Prog. Polym. Sci.* **2001,** *26*, 605-665.
48. Kurecic, M. S., M.; Stana, K., UV poly of Nisopropylacrylamide hydrogel. *Materials and technology* **2012,** *46*.

CHAPTER II – Water Structure and Mobility in Copolymer Galactose-Based Glycohydrogels

2.1 Introduction

Although swelling properties are often examined in existing glycohydrogel literature, limited studies have been performed to characterize physicochemical properties associated with glycohydrogels. The most notable works that probed the effects of swelling properties and water structuring were performed using various lactose-containing acrylamide monomers.[1, 2] Specifically, Roger et al. found that incorporating a small amount of *N*-acryloyl lactosamine in polyacrylamide hydrogels decreased the amount of free water measured via NMR.[1] Furthermore, the abundance of water molecules in high water content hydrogels has been shown to promote the formation of water clusters, which limit hydrogen bonding to the polymer network.[3, 4] Therefore, in addition to the availability of hydrogen-bonding groups, the overall hydrophilicity of the hydrogel network must be considered when analyzing the organization of water at the polymer interface.

Several studies have demonstrated that the inclusion of hydrophobic components can promote structural water formation and retard diffusional behavior of molecular water around hydrophilic groups.[5-7] Zhou et al., however, found no difference in bound water levels for copolymer hydrogels containing a lactose-containing acrylamide monomer and N-isopropylacrylamide (NIPAM) as a function of copolymer composition.[2] pNIPAM has a lower critical solution temperature (LCST) of 32°C. Hydrogels were characterized below the lower critical solution temperature (LCST) and therefore would have been in their most favorable hydrophilic morphology. The lack of bound water

variation may be the result of limited hydrophobicity. Thus, there is a need to understand the range of hydrophobicity necessary to promote water structuring in saccharide-containing copolymer hydrogels to enable the improved design of glycohydrogels for relevant biomedical and personal care applications. In this study, we have chosen to incorporate siloxane-containing acrylamide monomers to explore the extremes of amphipathic balance. The inclusion of siloxane moieties has an additional benefit for biomedical applications, due to the high oxygen permeation and bioinert character of siloxane polymers.

Acrylamide monomers with stereospecific galactose pendant groups were synthesized via a glycosylation reaction. A statistical design of experiments approach was taken to determine the effect of amphipathic ratio and crosslink density on water content and structural water composition in glycohydrogels consisting of 2′-(2,3,4,6–β-D-galactosyloxy)acrylamide (GalEAm). Copolymer hydrogels with hydrophobic components, consisting of acrylamide segments with a pendant siloxane group, were synthesized via UV-initiated free-radical polymerization in dimethyl sulfoxide (DMSO). Analogous dimethyl acrylamide (DMA) copolymer hydrogels were synthesized as a less hydrophilic reference system. Select polymer systems using experimentally determined swelling and hydrogel composition values to elucidate the diffusional properties within varying hydrogel architectures further.

It is important to acknowledge that all molecular simulations were performed by the Khare Research Group in the Department of Chemical Engineering at Texas Technical University. Analysis and writing of both experimental and simulation results were performed collaboratively through many discussions and written drafts.

2.2 Experimental

2.2.1 Materials

The following reagents and solvents were used as received from the supplier, *N,N'*-methylene bisacrylamide, 99% (BIS) (Sigma); 3-acrylamidopropyltris(trimethyl siloxy)silane, tech-95 (ATris) (Gelest); and anhydrous dimethyl sulfoxide, 99.8% (DMSO) (Alfa Aesar). *N*, *N*-dimethyl acrylamide, 99% (DMA) was purchased from Sigma-Aldrich and, before use, the inhibitor was removed via vacuum distillation. Irgacure 2959 was donated by BASF Chemical. Quartz plates (25.4mm^2 x 1mm) were purchased from TED Pella, shim stock (0.762 mm) was purchased from Precision Brand Products, and borosilicate glass culture tubes (5mL) were purchased from Fisher Scientific. The deacetylated glycomonomer, 2′-acrylamidoethyl-β-D-galactopyranoside (GalEAm), was synthesized according to a previously reported procedure.[8]

2.2.2 Design of experiments

A statistical design of experiments (DOE) approach was taken to elucidate the effect of crosslinker concentration and amphipathic balance on equilibrium water concentration (EWC) and bound water for two hydrophilic monomers (GalEAm and DMA), which exhibit drastically different hydrogen bonding potentials. Two independent two-factor three-level full factorial experiments with three replicates were conducted for the two hydrophilic monomers. Both designs were randomized before implementation and data analyzed in Minitab 17. Three crosslinker (BIS) concentrations (10, 15, and 20 mol%) and three hydrophobic (ATris) to hydrophilic molar feed ratios (10:90, 20:80, and 30:70) were specified.

2.2.3 Experimental sample preparation

2.2.3.1 Synthesis of linear polymer models

Linear copolymers with three hydrophobic to hydrophilic monomer feed ratios (10:90, 20:80, and 30:70) were prepared. Note that it was found that the hydrophobic monomer was incorporated at a lower level in the polymer than in the feed, so a naming convention based on the experimentally determined polymer composition was adopted. Linear polymers are denoted as pmol%hydrophilic monomer (i.e., p92DMA is a copolymer containing 8 mol% ATris and 92 mol% DMA, determined via ^{1}H-NMR). Stock solutions of monomer and initiator were prepared using anhydrous DMSO and were diluted to achieve the desired formulation with a final volume of 1 mL. Monomer (1M total hydrophobic and hydrophilic) and initiator (0.05 M) concentrations were held constant for all formulations. Due to oxygen sensitivity, all reactive formulations were purged with ultra-high purity nitrogen for 40 mins before polymerization in a culture tube. Once in the dry box, the reactive mixtures were polymerized via free radical polymerization by exposing to UV-light (38 mW/cm2) (Omnicure 2000, 200W lamp) for 3 minutes. After polymerization, polymers were extensively dialyzed against water followed by MeOH for three days each to remove DMSO and unreacted starting materials.

2.2.3.2 Synthesis of hydrogel copolymer networks

Copolymer hydrogels were synthesized using an additional stock solution containing BIS and following the same formulation protocol as the linear polymers. A similar naming strategy to that of the linear polymers was used where “p” is replaced by “h” to indicate hydrogel, followed by mol% hydrophilic monomer incorporated in the linear system, and the mol% BIS in the feed (i.e., h92DMA10BIS is a hydrogel

containing 8mol% ATris, 92 mol% DMA, and 10 mol% BIS). Nitrogen purged formulations were used to prepare hydrogels in an inert atmosphere using a mold consisting of a Teflon spacer (762 μm) sandwiched between two quartz plates. After polymerization, the molds were disassembled and the hydrogels released from the substrate by swelling in deionized water. Freestanding hydrogel films were first soaked in deionized water than in MeOH each for three days with daily water exchanges to remove the organic solvent and any unreacted monomer. Gravimetric analysis of dried residue from the first wash with water and MeOH showed negligible residual solids (< 1%).

2.2.4 Experimental characterization

2.2.4.1 Proton nuclear magnetic resonance spectroscopy

Linear copolymer composition was calculated using ^{1}H-NMR spectra collected on a Bruker 600 MHz using an optimized T_1 relaxation time for linear DMA and GalEAm copolymers with an average of 254 scans. Integration of specified proton shifts was analyzed to determine hydrophilic monomer inclusion. For the DMA copolymers, the silyl-methyl protons of ATris were integrated and assigned an area of 27. The DMA methyl protons were directly integrated and divided by six. The percent inclusion of DMA was calculated from the ratio of DMA methyl protons to Silyl-methyl protons. For the GalEAm copolymers, the anomeric proton at 4.54ppm was assigned an area of 1. The ATris silyl-methyl protons were directly integrated and divided by 27. GalEAm inclusion was calculated from the ratio of anomeric protons to silyl-methyl protons.

pDMA , ^{1}H NMR (600 MHz, DMSO-d_6 w/o TMS): δ [ppm] 3.17 (d, 2H-3), 2.79 (br, mt, 6H-7). 2.39 (br, H-2, 2'), 0.38 (s, 2H-5), and 0.08 (s, 27H-6). **Note:** The broad peaks between δ_H 1.75 to 1.00 ppm correspond to the protons of the polymer backbone

(H-1, 1') and ATris (2H-4). [^{1}H NMR spectra, Supporting information, Figure A.1].

pGalEAm , ^{1}H NMR (600 MHz, DMSO) δ 7.44 (br, 1H-3,3'), 5.10, 4.92 (br, 3H-11,12,13), 4.55 (s, 1H-10), 4.20 (br, s, 1H - 14), 3.69, 3.16, 3.09, (br, s, s,s, 7H-15, 8, 9), 0.40 (s, 2H-6), 0.08 (s, 27H-7). **Note:** The broad peaks between δ_H 2.20 to 1.00 ppm correspond to the protons of the polymer backbone (H-1, 1', 2, 2') and ATris (2H-4). [^{1}H NMR spectra, Supporting information, Figure A.2].

2.2.4.2 Thermogravimetric analysis (TGA)

All TGA profiles were collected with a TA Instruments TGA Q500 under nitrogen using a platinum pan. Thermal stability of linear homopolymers and copolymers comprised of GalEAm and ATris was determined with a temperature ramp test from 25 °C to 600 °C (10 °C/min). EWC was measured using a temperature ramp protocol (10 °C/min) from 25 °C to 200 °C. All samples were run in triplicate. The percentage of water loss was calculated using Equation 1, where W_o is the sample weight upon full saturation, and W_f is the final sample weight after dehydration. Samples were cut using a 0.25in diameter punch, and surface water was removed by lightly blotting with a Kimwipe® before testing. A gravimetric technique was used to confirm the TGA results

$$EWC = \frac{W_o - W_f}{W_o} x\ 100 \quad \text{..... Equation 2.1}$$

2.2.4.3 Differential scanning calorimetry (DSC)

All DSC profiles were collected with a TA Instruments DSC Q100 using a low volume hermetic pan with a small hole punched in the lid. The glass transition temperature of linear polymers was determined with a heat/cool/heat cycle at 10 ºC/min for GalEAm and DMA copolymers from 0 °C to 200 °C and 0 °C to 120 °C respectively. Structural water content was measured using a modification of the procedure reported by

Tranoudis et al.[9] Samples were prepared using a 3 mm diameter punch, surface water was removed by lightly blotting with a Kimwipe®, and the sample was sealed in a small volume hermetic pan (sample weight between 4 - 5 mg). DSC thermograms were obtained using a ramp rate of 1 °C /min,; sampleswere cooled to -40 °C, isothermally held for 2 min, and heated to 25 °C. The enthalpy of free water (Q_{FR}) plus restricted water (Q_R) was calculated by integrating the endothermic peaks for GalEAm and DMA copolymers from ⁻20 °C to 5 °C and ⁻10 °C to 5 °C, respectively, using the TA analysis software. The measured heat of fusion of pure water (Q_p, 330 J/g) was used in Equation 2 to calculate the fraction of free and restricted water (X_{FR+R}). Bound water (X_B) was then calculated using Equation 3 where the fraction of free and restricted water was subtracted from the EWC measured via TGA.[10]

$$X_{FR+R} = \left(\frac{Q_{FR}+Q_R}{Q_P}\right) * 100 \quad \text{Equation 2.2}$$

$$X_B = (EWC - X_{FR+R}) \quad \text{Equation 2.3}$$

2.2.4.4 Dynamic vapor sorption analysis (DVS)

The relative percentage of dehydration was measured using a TA Instruments DVS q5000. Hydrated samples were cut using a 6.35mm diameter punch and surface water was removed by blotting with a Kimwipe® before loading onto a quartz pan. Dehydration profiles were generated by monitoring the relative weight change of a sample isothermally held at 34 °C in 35%, 60%, and 95% relative humidity (RH) environments under a constant nitrogen flow rate of 9 mL·min-1. Hydrated sample thicknesses were measured using a Keyence VHX 600 optical microscope with an inline light source at 100x magnification. The diffusion constants associated with desorption from a fully hydrated hydrogel were calculated from the dehydration profiles obtained at

constant relative humidity. From desorption profiles and thicknesses measured in the hydrated state, the diffusion coefficients were calculated using Equation 4.[11, 12]

$$\frac{M_t}{M_\infty} = \frac{4}{d}\sqrt{\frac{Dt}{\pi}} \quad \text{Equation 2.4}$$

Where M_t is the mass absorbed at time t, M_∞ is the mass at equilibrium obtained at full desorption, D is the diffusion constant, d is the film thickness, and t is time. The slope of M_t/M_∞ vs. $t^{0.5}/d$ at values of $M_t/M_\infty < 0.4$ was used to calculate the diffusion constants. It is important to note that because the diffusivity through a polymeric film is highly influenced by sample thickness, the average edge on thickness taken from three fully saturated samples were measured before testing.[11]

2.2.5 Simulation details

Molecular dynamics (MD) simulations using atomistic models of hydrogel systems were performed using the LAMMPS package[13] with a timestep of 1 fs. The van der Waals and the electrostatic interactions were calculated explicitly up to 12 Å. Beyond the cut-off (12 Å), the van der Waals interactions were approximated using the tail corrections, while the electrostatic interactions were calculated using the particle-particle particle-mesh (PPPM) algorithm.[14] In all of the simulations, the temperature and pressure of the system were maintained at the desired value (298 K and 1 bar, respectively) using Nosé-Hoover thermostat and barostat.[15, 16] To obtain good statistics, the calculations were repeated in three replicas, and all the error bars represent standard deviation across all the structures. Details about the simulation systems and force field implemented are described below.

In concurrence with the experimental systems, two types of crosslinked networks (hGalEAm-ATris and hDMA-ATris) were studied in simulations. Model systems of the networks were investigated only at 10 and 20 mol% ATris content to most closely match the experimentally observed incorporation of the hydrophobic monomer in the polymer. The in-silico structures were built using the respective composition of the network and water content at equilibrium, calculated from experiments. The simulated annealing polymerization algorithm was employed to create the network structures. [17, 18] For this purpose, monomer mixtures containing all the components in the desired fraction were first equilibrated. Following the equilibration, the reacting monomers that were spatially closest were identified using a simulated annealing optimization algorithm and then connected to form the network structure. The final systems so obtained were then relaxed by cooling them from 400 K to 340 K and 340 K to 300 K in steps of 5 K/ns and 10 K/ns, respectively. Production runs were performed on relaxed structures for a period of 40 ns and the relevant quantities of interest were calculated. Specific procedures for calculating the desired properties are explained in the results and discussion section.

All the parameters necessary to describe intermolecular and intramolecular interactions involving GalEAm, DMA, and BIS monomers were obtained from the general AMBER force field (GAFF).[19, 20] The SPC/E model[21] was used to represent the water molecules and the SHAKE algorithm[22] was additionally used to constrain the bond lengths and bond angles at their respective equilibrium values. The ATris monomer was represented by combining two sets of force-field parameters, which are (1) GAFF for carbon, oxygen, and hydrogen atoms and (2) values that were optimized based on COMPASS[23] and the united atom representations of polydimethylsiloxane (PDMS) and

polyhedral oligomeric silsesquioxanes (POSS) for interactions due to silicon atoms.[24-27] Specifically, all the intramolecular parameters (bonds, angles, and dihedrals) involving Si atom were obtained from united atom force field values developed for PDMS polymer and POSS molecule. In the case of non-bonded interaction parameters (ϵ,σ), the values from the COMPASS force field were initially used and optimized to reproduce the experimental density values of chemical compounds that structurally and chemically resemble the ATris monomer. For the sake of clarity, the force field parameters pertaining to ATris and a description of the optimization procedure are reported in the Appendix (A.1 and A.2).

2.3 Results and discussion

2.3.1 Composition and thermal properties of linear GalEAm and DMA copolymers

Linear homopolymers (GalEAm, DMA, and ATris) and copolymers (GalEAm-ATris and DMA-ATris) were prepared by photo-initiated free radical polymerization to determine copolymer composition and thermal properties. Table 2.1 summarizes copolymer composition determined via ^{1}H-NMR as well as the T_gs obtained from DSC and simulations. Incorporation of ATris in the copolymer is lower than the feed ratio, with decreasing incorporation at higher feed ratios for both the GalEAm and DMA systems (spectra are shown in Appendix Figures A.1 and A.2).

Table 2.1

Summary of linear polymer characterization exhibiting hydrophilic monomer inclusion and glass transition temperatures (Tg).

Feed Ratio (hydrophilic : ATris)[a]	**Hydrophilic monomer (%)[b]**	**Tg (°C) (DSC)**	**Tg (°C) (Simulation)**
0 : 100	-	42.8	-
100 GalEAm : 0	-	156	193.7 ± 5.4
90GalEAm : 10	92.0	150.6	-
80GalEAm : 20	85.1	148.9	-
70GalEAm : 30	84.4	147.3	-
100 DMA : 0	-	114	225.2 ± 30.5
90 DMA : 10	92.3	101.4	-
80 DMA : 20	87.0	79.1	-
70 DMA : 30	84.3	72.3	-

[a] Initial molar feed ratio of comonomers. [b] Mole percentage of hydrophilic copolymer composition, determined by ^{1}H-NMR.

Lower ATris inclusion is attributed to steric bulk polarity and miscibility differences between ATris, GalEAm, and DMA monomers. Similar differences in comonomer inclusion have been reported in glycopolymers containing aromatic[28] and NIPAM[2] comonomers. Furthermore, the disparity between hydrophilic and siloxane-containing vinyl monomers has been shown to impact compatibility; this can be mitigated by using an acrylamide monomer and additional amide groups.[29, 30] In our copolymer systems adequate levels of ATris incorporation are achieved to allow comparison of

properties as a function of composition. Measured T_gs of the GalEAm, DMA, and ATris homopolymers are 156°C, 114°C, and 42.8°C, respectively. The T_gs of GalEAm and DMA copolymers decrease with higher ATris inclusion, as expected (DSC traces shown in Appendix Figure A.4). Measured T_gs show deviation from those predicted by the Fox equation (Figure 2.1), particularly for the GalEAm system where T_gs are substantially higher than predicted. This indicates limited miscibility of the comonomers due to their great difference in polarity.[31]

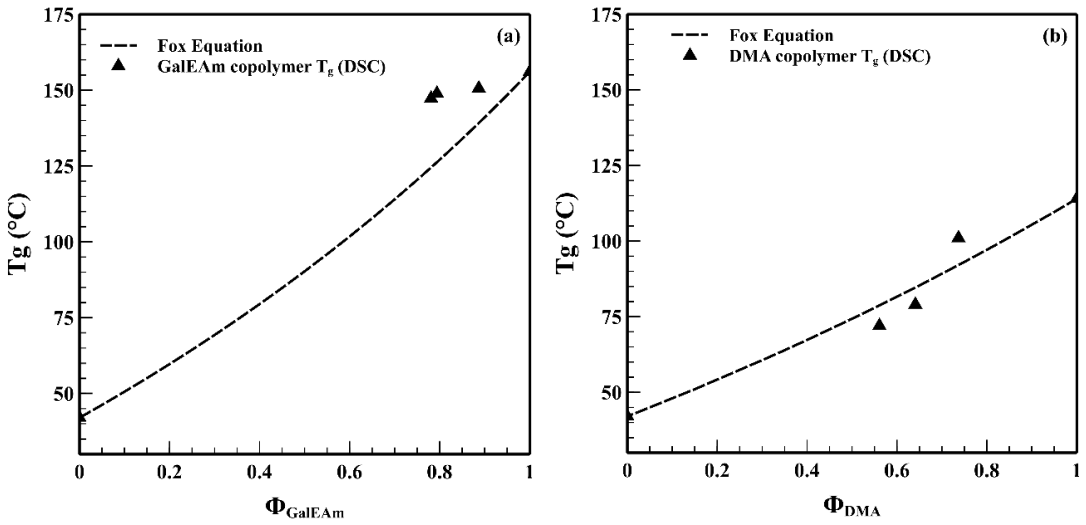

Figure 2.1 Measured Tgs for (a) GalEAm and (b) DMA copolymers as a function of weight fraction (Φ) of hydrophilic monomer. Deviation from Fox equation prediction is attributed to limited miscibility of comonomers.

The force-field parameters and the model structures were validated by calculating the glass transition temperature from simulations and comparing with the experimental data. For this purpose, only linear GalEAm and DMA homopolymers were considered. As described in the simulation details section, the linear homopolymer structures were also built using the simulated annealing polymerization technique. The glass transition

temperatures were then measured by cooling the systems from T = 750 K to T = 170 K in steps of 20 K. After each temperature step, the systems were maintained at constant temperature and pressure for a period of 2 ns and the specific volumes at that temperature were then measured as the average of values from the last one ns of the simulations. From the specific volume – temperature data, Tg is determined as the point of intersection of linear fits to rubbery and glassy regions.

For ATris homopolymer, since the non-bonded interaction parameters were specifically optimized to reproduce the density values of ATris-like compounds, separate simulations to calculate the glass transition temperature were not performed. It can be seen that the Tg calculated from simulations differ by approximately 38 K and 111 K from those of experiments for GalEAm and DMA linear polymers, respectively. Similar observations have been reported in the literature for a wide range of systems, such as asphalt,[32] ionic liquids,[33] and crosslinked epoxies[18] that differ in their molecular weight, connectivity, and interactions. Specifically, differences of 113 K (asphalt), 77 K (ionic liquids), and 27 K (epoxies) were observed and attributed to significantly faster cooling rates used in simulations compared to experiments. William-Landel-Ferry (WLF) equation, which characterizes the temperature dependence of relaxation time, has been used previously to estimate the expected shift in Tg due to the differences in cooling rates.[32-35] Given the need for system-specific parameters in the WLF equation, we have not quantified these differences for our hydrogel systems. However, we note that with the orders of magnitude difference in the cooling rates used in this work (simulations ~ 10^{10} K/min and experiments ~ 10 K/min), the observed shift in T_g is expected.

TGA curves, in Figure 2.2, for linear ATris, GalEAm and DMA homopolymers and copolymers show different degradation behavior, attributed to differences in hydrogen bonding capability and intermolecular interactions between pendant groups. GalEAm copolymers exhibit an additional weight loss event slightly above 100°C not observed in GalEAm homopolymers (Figure 2.2.a). This is attributed to volatilization of tightly bound environmental water, suggesting that incorporation of ATris promotes hydrogen bonding between water molecules and hydrophilic sites of the polymer. Furthermore, the bulkiness of GalEAm interrupts the interaction of neighboring amine groups resulting in a two-stage degradation event of the acrylamide backbone at high temperatures similar to that observed by Silva et al.[36] In the DMA copolymers (Figure 2.2.b) incorporation of ATris results in a two-stage degradation event, with a decrease in temperature onset from 323°C for p(100DMA) to 230°C for p(84DMA). The initial weight loss, associated with the volatilization of water below 100°C, decreases with ATris incorporation (11% for p100DMA, 4% for p92DMA, and 8% for p84DMA). Furthermore, there is no remaining residue after degradation for p100ATris homopolymer (Figure 2.2.b) whereas an increase in the remaining residue is observed for p92DMA (18%) and p84DMA (11%). Yokota et al. report a similar behavior for acrylamide polymers containing methyl-bis(trimethylsiloxy) pendant groups tested under nitrogen.[29] They suggest the possible formation of a silicate structure at high temperatures resulting from recombination of cleaved silicone bonds,[29] a behavior they first report observing during silicone degradation events in an Ar gas plasma.[37] For DMA copolymer hydrogels, greater phase separation and siloxane inhomogeneities, visually observed, may allow for the formation of a similar silicate structure.

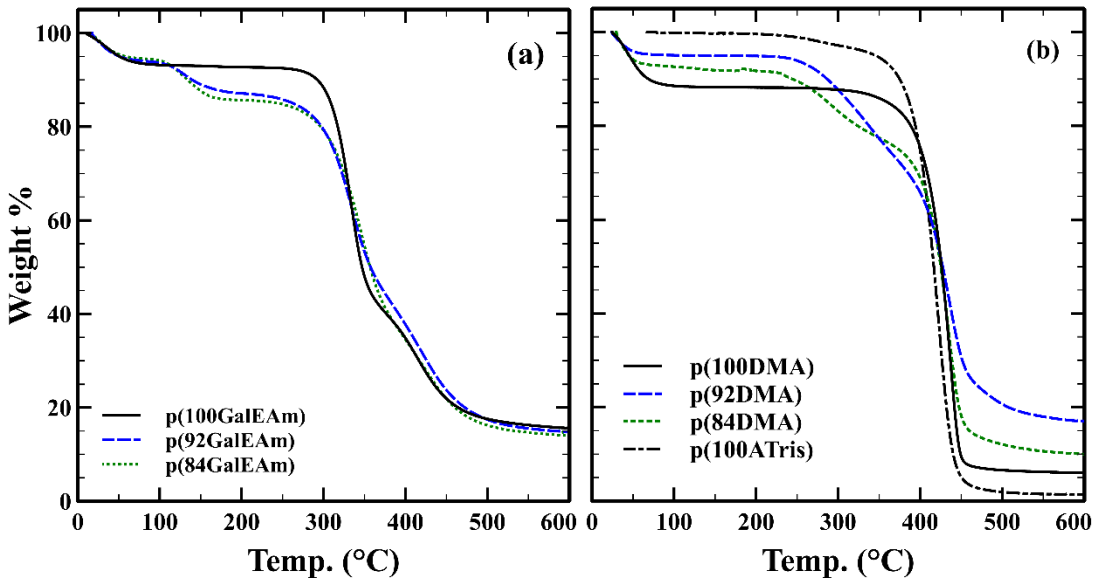

Figure 2.2 Incorporation of ATris results in (a) increased bound water concentration in pGalEAm copolymers shown by the weight loss slightly above 100 °C, and (b) the onset of degradation for pDMA copolymers.

2.3.2 Optical Appearance of GalEAm and DMA Copolymer Hydrogels

Visual appearance and opacity of hydrogel compositions at full saturation are shown in Figure 2.3. The GalEAm copolymer hydrogels appear transparent, except at the highest ATris and BIS loadings where small opaque regions are observed. These are attributed to phase separation resulting from the extreme difference in hydrophilicity of the two monomers, consistent with the lack of miscibility indicated by the deviation from the Fox equation prediction of Tg. The DMA copolymer hydrogels exhibit an increase in opacity with increasing ATris and BIS loading. It has been shown in similar acrylamide hydrogels that increasing crosslink density distorts the polymer network resulting in increased opacity due to spatial inhomogeneity.[38, 39] This is apparent in the DMA hydrogels containing low ATris loading where opacity increases with high BIS

concentration. Higher ATris content results in increased opacity due to phase separation of the hydrophobic component. Suggesting the opacity of the resultant film is determined by the interplay between hydrophobic content and crosslinking concentration.

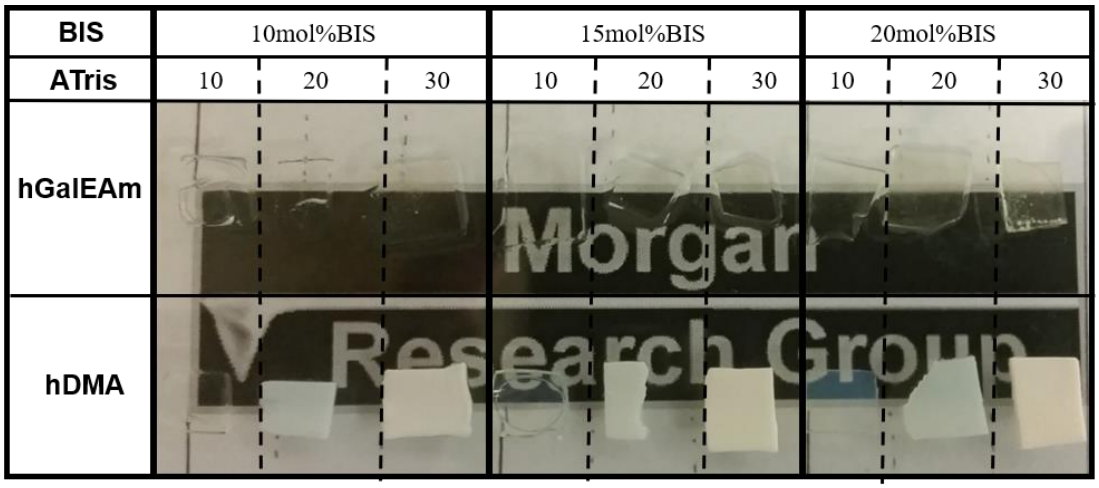

Figure 2.3 Visual properties of hydrogels with different molar BIS and ATris feed ratios. GalEAm copolymers show visible phase separation at high ATris and BIS loading and DMA copolymers are opaque at all but the lowest crosslink densities.

2.3.3 EWC in GalEAm and DMA Copolymer Hydrogels

As discussed in the experimental section, a statistical design of experiments approach was taken to determine the significant variables and their interactions on EWC and bound water using a 2^3 full factorial design, and the resulting ANOVA from the general regression is shown in the Appendix (Table A.2). EWC in GalEAm and DMA hydrogels of all compositions is high, ranging from 65 to 90% (Figure 2.4). As expected, EWC decreases with increasing ATris and BIS loading for the GalEAm copolymer hydrogels. The DMA copolymer hydrogels, on the other hand, exhibit no clear trend in EWC with respect to BIS or ATris loading, which is contrary to expectation. According to the ANOVA, both models exhibit statistical significance ($p < 0.05$), although there are

differences in the variables determining EWC for the two systems. In GalEAm hydrogels, both ATris and BIS loading significantly affect EWC ($p<0.5$), but there is no apparent interaction between the two variables (Table A.4.a). When the interaction term is significant, interaction plots exhibit non-parallel curves, not observed in Figure 4a. In the DMA hydrogels, ATris loading and the interaction term show statistical significance ($p<0.05$) in determining EWC (Table A.4.b).

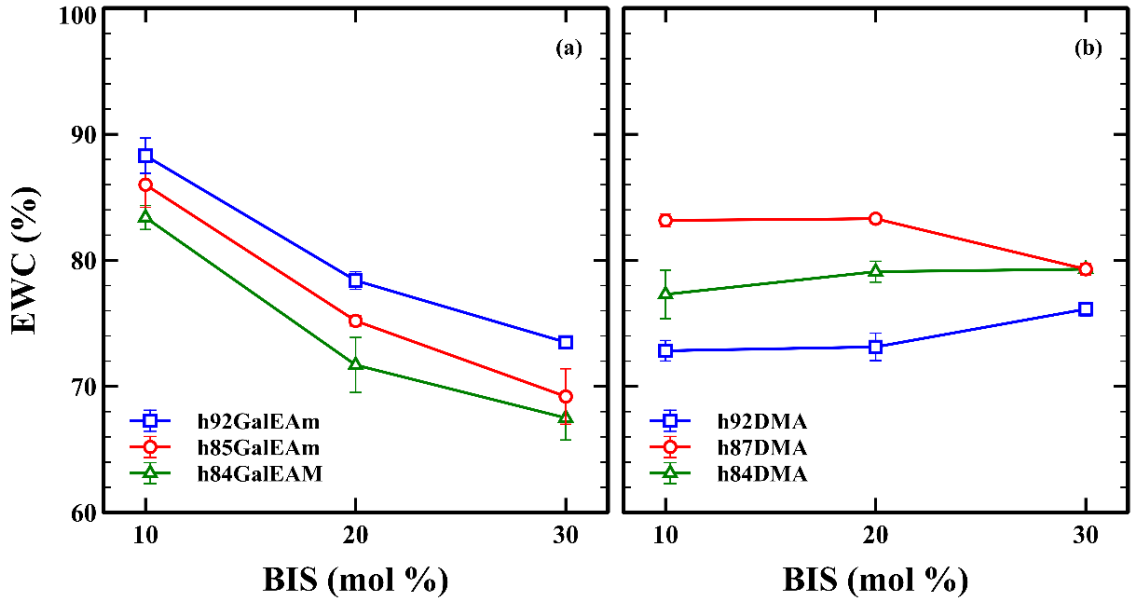

Figure 2.4 (a) hGalEAm copolymer hydrogels exhibit a decrease in EWC with higher BIS and ATris loading whereas (b) hDMA copolymer hydrogels show no consistent trend.

2.3.4 Measuring and defining bound water for experimental and simulation approaches

The bound water content in saturated hydrogels was determined experimentally using EWC and heat of fusion from DSC (characteristic curves are shown in Figure 2.5). As described in the introduction, water exhibits differences in melting behavior

depending on the degree of hydrogen bonding with polymer sites, captured upon freezing. Although all DMA and GalEAm hydrogels exhibit a free water peak at 0°C, only GalEAm hydrogels with 20 mol% BIS exhibit an isolated, restricted water peak (Figure 2.5.c), suggesting that restricted water content is dictated not only by hydrogen bonding sites but also by hydrophobic loading and crosslink density.

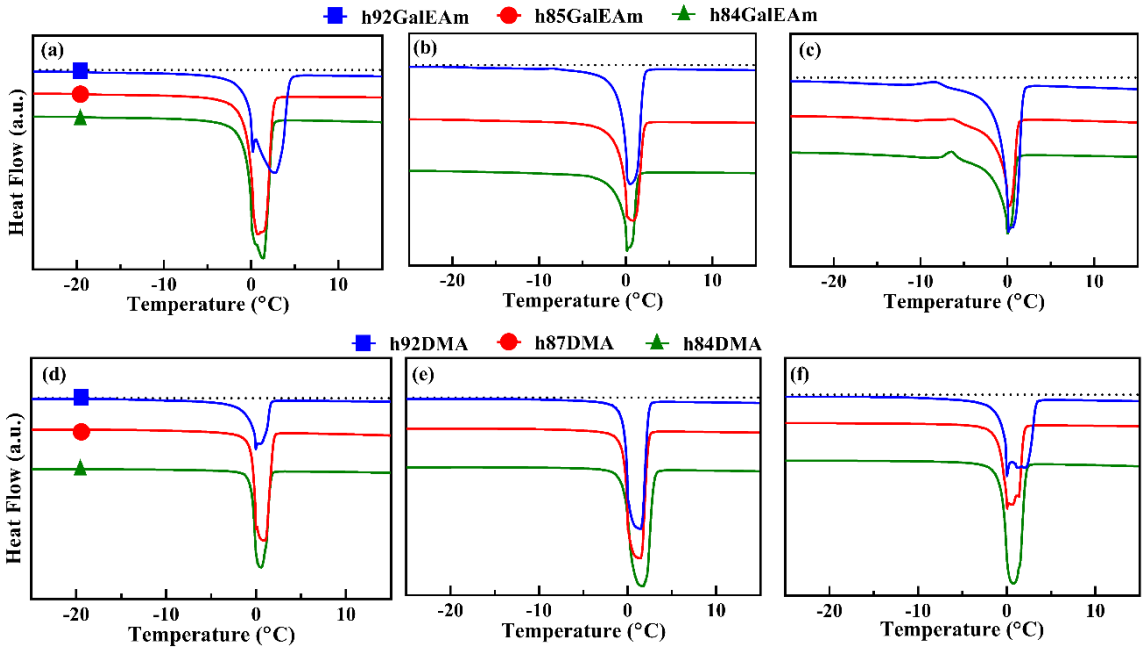

Figure 2.5 Representative endotherms for h(GalEAm) (top) and h(DMA) (bottom) copolymer hydrogels, containing 10 (a,d), 15 (b,e), and 20 mol% BIS (c,f) obtained by DSC. Hydrophilic monomer composition specified in plot key. In general, GalEAm hydrogels show greater melting point depression and more prominent low-temperature shoulder peaks than DMA hydrogels.

In simulations, the population of bound water was measured directly by comparing the translational mobility of bulk water molecules with the translational mobility of water molecules in various hydration shells of the hydrogen bond forming

polymer groups (OH and CONH groups of GalEAm, ATris, and BIS). Based on the reduced translational mobility exhibited by the water molecules in the polymer hydration layers, a cut-off distance was identified for each polymer group (see Figure A.5and Appendix A.3 for details about the MSD calculations). All the water molecules within the cut-off are classified as bound water. The water molecules within the first hydration layer of the bound water are classified as restricted water,[40] while the remaining water molecules are tagged as free water.

2.3.5 Dependence of bound water on various factors such as hydrogel composition and swelling

2.3.5.1 Bound water population with respect to EWC

The amount of water at equilibrium in the hydrogel is known to affect its dynamics,[7, 41] therefore the correlation of bound water fraction to EWC was examined, shown in Figure 2.6 (the inset shows the average hydrogen bond lifetime, the significance of which is explained in detail in the next section). For the GalEAm hydrogels, bound water appears to decrease with respect to EWC in both experiment and simulation. In the DMA system, simulation indicates a small increase in bound water with increased EWC and higher standard deviations than those observed for GalEAm. Experimental data for DMA show large variations in bound water and no clear trend with EWC. The higher correlation of bound water with EWC in GalEAm hydrogels is attributed to the greater abundance of hydrogen bonding groups in the pendant saccharide moiety. We note that, although bound water population identified both from experiments and simulations are of similar magnitude, especially with respect to GalEAm hydrogels, an exact quantitative agreement is not observed. These discrepancies are due to differences in measurement

techniques discussed previously and persist throughout all examination of bound water populations within varying hydrogel compositions. Nevertheless, we focus on understanding the mechanism of the hindered mobility of water molecules. Therefore an exact quantitative agreement is not as important as the qualitative trends.

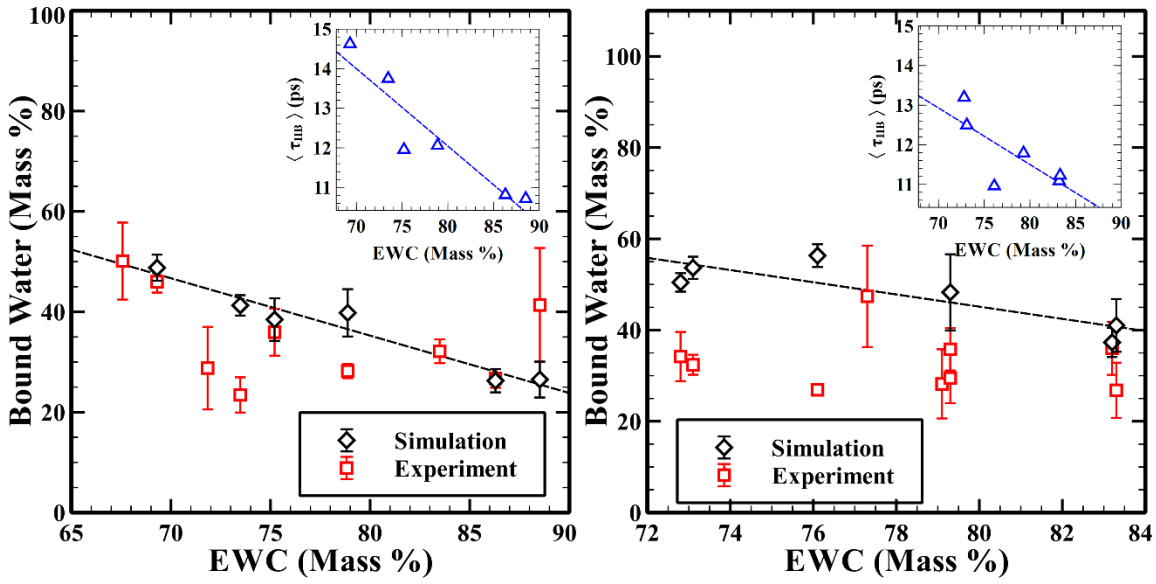

Figure 2.6 Variation of bound water with respect to EWC for (a) GalEAm and (b) DMA hydrogels. Both GalEAm and DMA hydrogels show a decrease in bound water with increasing EWC in simulations, with the trend being more prominent in GalEAm gels. Inset of the figures shows the lifetime of water-polymer hydrogen bonds (averaged between all hydrogen bond forming sites on the polymer) calculated from simulations. A linear fit to simulation data (dotted line) is shown to guide the eye.

2.3.5.2 Effect of hydrophobicity and crosslink density on bound water

The bound water population is influenced by hydrogel composition and structure as well as EWC; therefore the effects of ATris and BIS loading were studied experimentally and by simulation, summarized in Figure 2.7. Although hGalEAm

exhibits large experimental variation, especially at low ATris loading, it is clear that the samples with higher ATris and BIS loadings contain a higher fraction of bound water for both experiments and simulations. Despite variation in the GalEAm hydrogel data, the ANOVA exhibits statistical significance ($p < 0.05$), shown in supplemental Table S4a, with statistically significant differences between means for bound water attributed to %BIS and the interaction term. The experimentally determined bound water values in DMA hydrogels exhibit considerable variation and the model is not significant ($p > 0.05$), (Appendix Table A.4.b). In simulations of DMA hydrogels, bound water values show higher variation and there is no statistically significant difference with respect to BIS loading. In contrast to the GalEAm hydrogels, higher bound water is observed at the lower level of the hydrophobic monomer in DMA hydrogels.

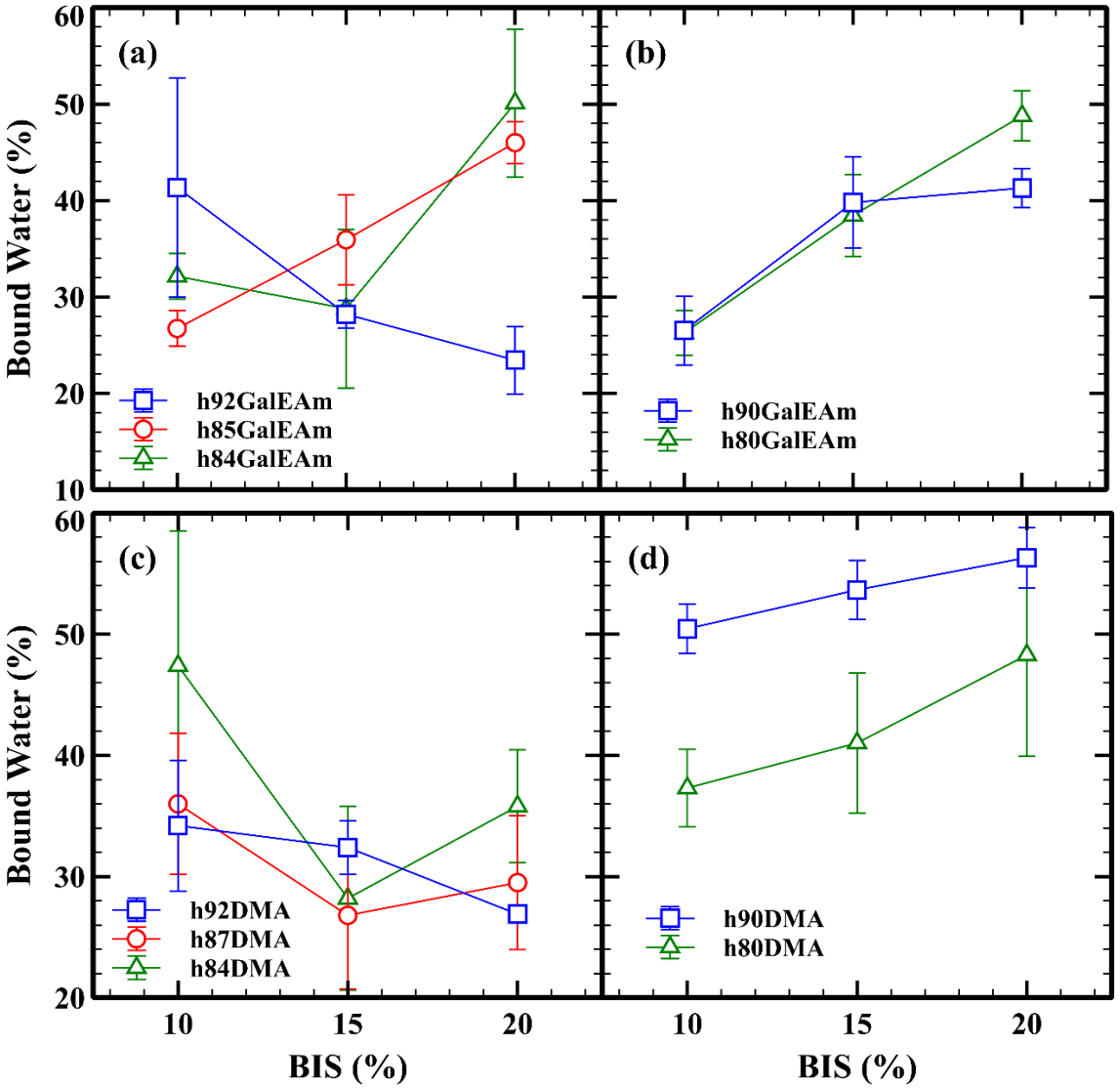

Figure 2.7 Bound water content calculated from experiments (left) and simulations (right) for hGalEAm (a,b) and hDMA (c,d) copolymer hydrogels. Copolymer composition for experimental and calculated values are reported. GalEAm copolymer hydrogels exhibit the highest bound water content at high BIS and ATris loading.

Based on these observations, the conclusions can be summarized as follows: (1) the bound water population is correlated to the EWC for both the hydrogels studied (Figure 2.6) and (2) correlation between bound water population and polymer

composition is observed for GalEAm gels while no such correlation is established for DMA hydrogels (Figure 2.7). The reasons for the above observations are explained in detail in the next section. Briefly, we propose that in addition to hydrogen bonding of water molecules with the polymer groups, their structural relaxation near hydrogen bonding sites should also be taken into consideration as it contributes significantly to water confinement effects,[42-44] which in turn determines the bound water population.

2.3.6 Comprehensive analysis of structural water relaxation modes around hydrogen bonding groups

To describe water mobility regarding structural water relaxation, the relative number of hydrogen bonds formed between water molecules and different hydrogen bonding groups were calculated for h80GalEAm20BIS, shown in Figure 2.8. The arguments presented here are also applicable to other hydrogels containing varying ATris and BIS loadings, which were studied but not reported. The hydrogen bonds were determined using geometric criteria.[45] Accordingly, a pair of molecules/groups are considered hydrogen bonded if all of the following conditions are satisfied (1) distance between the donor and acceptor heavy atoms (oxygen or nitrogen) is less than 3.5 Å, (2) distance between acceptor heavy atom and donor hydrogen atom is less than 2.5 Å, and (3) the angle formed by the acceptor heavy atom and the donor OH bond is less than 30°.

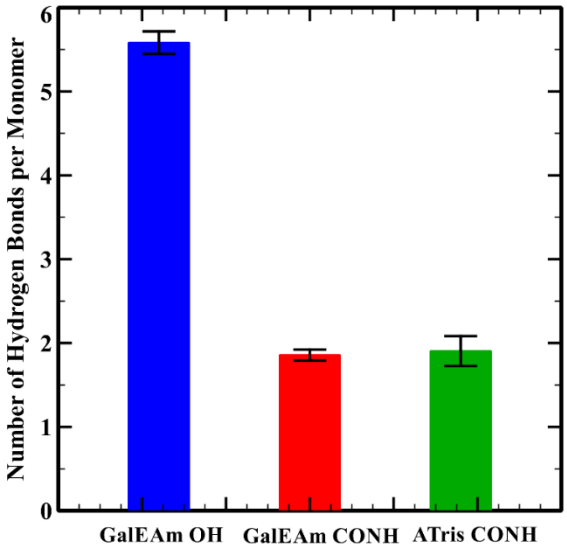

Figure 2.8 Number of water-polymer hydrogen bonds per monomer for h(80GalEAm20BIS).

From Figure 2.8, GalEAm-OH groups contain almost three times as many hydrogen bonds as compared to GalEAm-CONH and ATris-CONH groups. Although most of the water-polymer hydrogen bonds are formed with hydroxyl groups, these water molecules form a percolating network and are not bound. This conclusion is supported by the orientational relaxation of polymer-water hydrogen bonds, illustrated in Figure 2.9. The continuous correlation function (CCF) shown in Figure 2.9.a describes the lifetime of the hydrogen bonds while the intermediate correlation function (ICF), Figure 2.9.b, is related to the mobility of the water molecules. The CCF and ICF were calculated using the same procedure outlined by Mani et al.[7] Briefly, the correlation functions (both CCF and ICF) are defined as follows:[46]

$$C(t) = \frac{<h(0)h(t)>}{<h(0)h(0)>} \quad \text{Equation 2.5}$$

Here, the pointed angular brackets denote the ensemble average over all the hydrogen bonding pairs in the system and *h* is a binary variable that can take a value of either one or zero. Particularly, the variable h(t)=1 if a given pair of molecules identified as hydrogen bonding partners at time t=0 is also hydrogen bonded at time t. Based on the above definition, the CCF and ICF are calculated as follows. In CCF, the variable h(t) takes a value of one when a pair of molecules is continuously hydrogen bonded from time t=0 to time t. On the other hand, in ICF, the variable h(t) takes a value of one if a pair of molecules is hydrogen bonded at time t=0 and at time t irrespective of their state at intermediate times (i.e. the hydrogen bonds can break and reform at intermediate time).

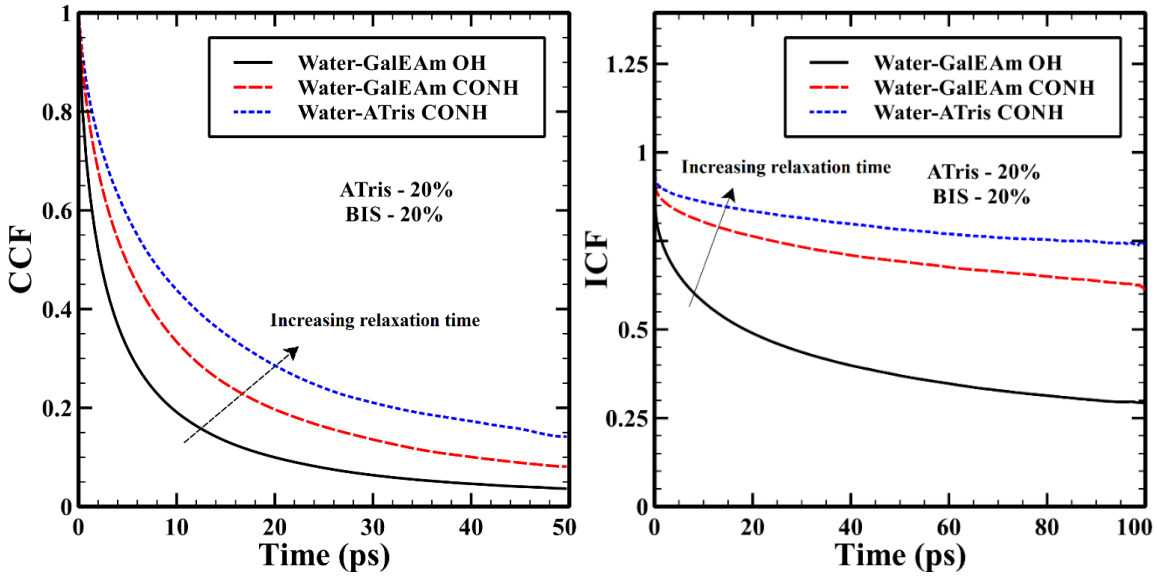

Figure 2.9 (a) Continuous correlation function (CCF) and (b) Intermediate correlation function (ICF) of the hydrogen bonds formed between water molecules and the polymer groups in GalEAm hydrogel with 20% ATris and 20% BIS loading.

From Figure 2.9, it is clear that the water-polymer hydrogen bonds relax at different timescales depending on the polymer groups. To quantify this effect, we have fit

both the CCF and ICF to Kohlrausch-William-Watts stretched exponential form,[47] defined as:

$$C(t) = \exp[-\left(\frac{t}{\tau}\right)^{\beta}]$$ ..... Equation 2.6

In this expression, β denotes the stretched exponent, while τ denotes the respective timescale associated with the correlation functions (lifetime for CCF and structural relaxation time for ICF). The hydrogen bonds formed by water molecules with the hydroxyl groups have a lifetime of ~5-7 ps (for all ATris and BIS loading studied) as determined from the CCF. On the other hand, the lifetime of hydrogen bonds formed between water molecules and GalEAm CONH groups is on the order of ~10-14 ps. The most stable hydrogen bond is observed between water and ATris CONH, which has a lifetime that is three times larger than the GalEAm OH-water hydrogen bonds (~16-22 ps). This observation supports our previous argument that the number of hydrogen bonds formed is not the only governing parameter that determines the distribution of bound water and that the structural relaxation of water near the specific sites on the polymer should also be considered. The structural relaxation of water-polymer hydrogen bonds is responsible for the observed decrease in bound water with an increase in equilibrium water content. Figure 2.6 inset shows the average lifetime of water-polymer hydrogen bonds (between all the hydrogen bonding groups in the polymer) with respect to EWC, which shows a decreasing trend similar to the variation of bound water with EWC. The GalEAm hydrogels show a broader range in the average lifetime of hydrogen bonds than observed for DMA hydrogels. These results show that the coupled hydrogen bond dynamics between water molecules and hydrogen bonding sites of the polymer dictate the bound water population, which in turn, is governed by various factors such as the fraction

of hydrophobic monomers in the network, the crosslink density, and the relaxation of the side-chain polymer group. The slow relaxation of water-ATris hydrogen bonds also explains the observed increase in bound water with the increase in the hydrophobic polymer composition (see Figure 2.7.a&b).

The lifetime of water-water hydrogen bonds show a similar trend to that of water-polymer hydrogen bonds (see Appendix, Figure A.5), i.e., water molecules in the vicinity of hydrophobic ATris groups exhibit the slowest hydrogen bond relaxation dynamics (~4-6 ps) at different hydrophobic loading and cross-linker density. An illustrative depiction of environmentally driven structural water relaxation modes between water-polymer hydrogen bonding events for GalEAm hydrogels are shown in Figure 2.10. The water molecules close to hydrophilic hydroxyl groups exhibit faster dynamics (~2.5-3 ps). A similar conclusion can also be drawn from the translational mobility of water in the hydration shell of the polymer (Figure A.6, Appendix). Similar observations are also reported in the literature[43, 48] and are associated with the limited number of hydrogen bonding partners available for water molecules near the hydrophobic groups.[44] The orientational and translational relaxation of water occurs by continually breaking the existing hydrogen bonds and forming new ones with the surrounding water/polymer groups. As the number of hydrogen bonding partners (both water and polymer hydrogen bonding sites) are limited near the ATris group due to hydrophobic fluctuations[49, 50], the structural relaxation of water is slower. Therefore, perturbation of the hydrophilic environment through the inclusion of ATris disrupts water-water clustering by inhibiting structural relaxation modes around hydrophilic groups as a result of kinetic entrapment (Figure 2.10.b).

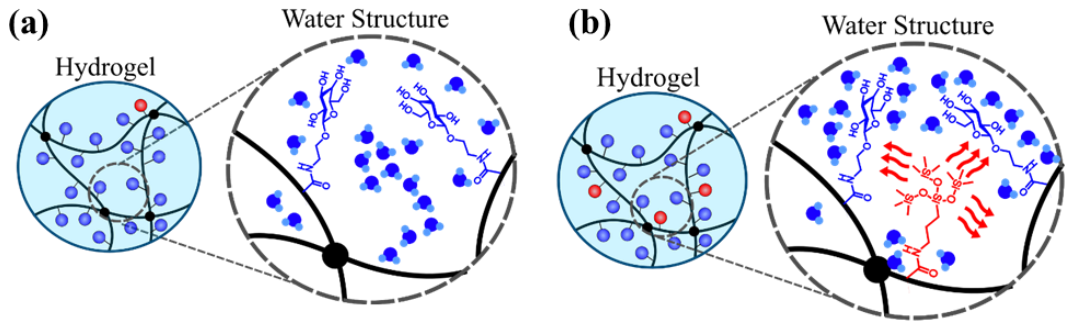

Figure 2.10 Illustration of environmental effects on structural water distribution in GalEAm hydrogels where highly (a) hydrophilic environments promote water clustering. (b) Hydrophobic environments promote bound water formation through disruption of water-water hydrogen bonding and inhibition of structural water relaxation dynamics between water-polymer hydrogen bonds.

2.3.7 Dehydration Characteristics

The effect of bound water concentration on diffusion coefficients in experimental systems was determined using DVS for GalEAm hydrogels with the lowest (23 ± 3.5%) and highest (50 ± 7.7%) measured bound water, associated with h92GalEAm20BIS and h84GalEAm20BIS respectively. For consistency, similar DMA hydrogel compositions were evaluated, h92DMA20BIS (26 ± 0.3%) and h84DMA20BIS (36 ± 4.6%). Reported in Table 2.2 are the hydrogel thicknesses at saturation and the summarized diffusion coefficients, which were calculated from the kinetic profiles (Figure 2.11) using the relationship defined in Equation 2.4. Diffusion coefficients were calculated within the Fickian diffusion regime (Mt/Meq <0.4) from the slope of Mt/Meq vs. t0.5/d.[11, 12] Film thickness can affect solute diffusion. Therefore saturated hydrogel thickness was measured immediately before testing (example cross-sectional images are shown in the

Appendix, Figure A.7). In relation to molded dimensions (762 μm), the thickness of the h92GalEAm20BIS increased whereas the thickness of h84GalEAm20BIS, h92DMA20BIS, and h84DMA20BIS decreased (Table 2.2). Furthermore, dimensional changes and thermodynamic transitions from a plasticized rubbery state to a glassy state during dehydration[51] can affect solute diffusion. However, by evaluating the surface desorption processes during the initial dehydration stages physical and thermodynamic changes to the hydrogels can be ignored, allowing the comparison of diffusion coefficients between hydrogel architectures and saturation environment.

Table 2.2

Summary of the changes in hydrogel thickness upon hydration and corresponding diffusion coefficients showing a slower rate of diffusion with an increase in bound water content and RH.

Sample	**Ave Hydrated Thickness (μm)**	**Diffusion Coefficient (cm^2*s^{-1}) ($x10^7$) at RH**		
		35%	**60%**	**95%**
h92GalEAm20BIS	935 ± 9	2.92 ± 0.37	1.61 ± 0.14	0.28 ± 0.0098
h84GalEAm20BIS	627 ± 75	2.10 ± 0.23	1.19 ± 0.11	0.203 ± 0.013
h92DMA20BIS	511 ± 26	1.51 ± 0.15	0.95 ± 0.11	0.166 ± 0.024
h84DMA20BIS	683 ± 15	2.06 ± 0.12	1.31 ± 0.031	0.204 ± 0.0049

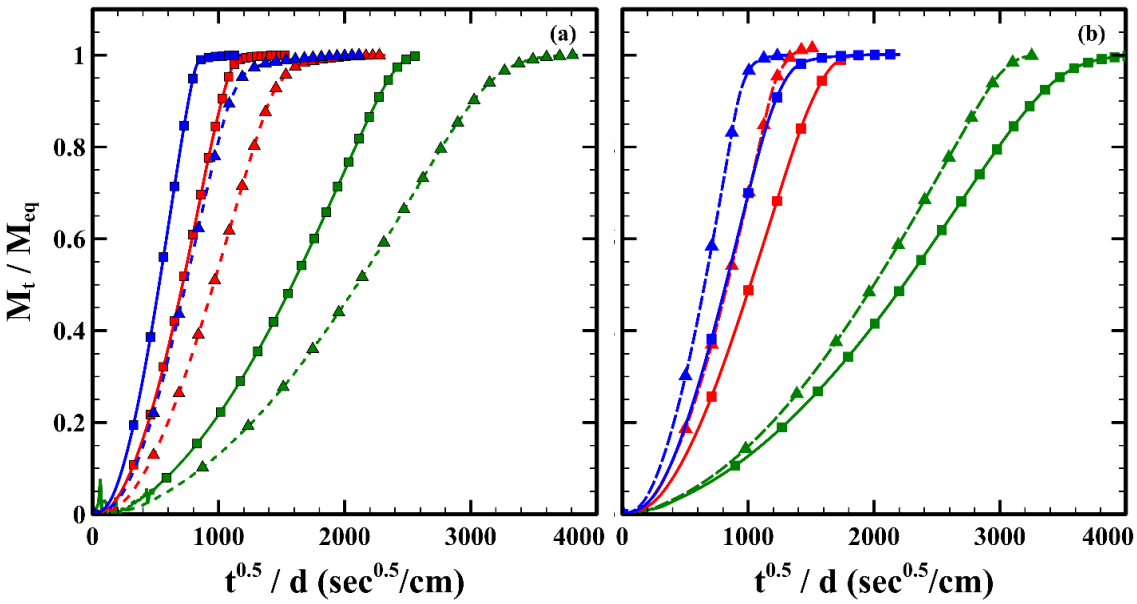

Figure 2.11 Diffusion kinetics profiles derived from dehydration profiles for 35%RH (blue), 60%RH (red), and 95%RH (green) for h(h-GalEAm20BIS) (square/solid line) and h(l-GalEAm20BIS) (triangle/dashed line). In general, a high saturation environment slows diffusion processes.

As expected, the time to dehydration, where M_t/M_{eq} plateaus as shown in Figure 11, is faster at 35% RH compared to 95% RH for both GalEAm and DMA hydrogels. Suppressed solute mobility by the high saturation environment overshadows the effects of network architecture, EWC, and bound water content, resulting in lower diffusion coefficients (Table 2.2). This is consistent with other reports on hydrogel systems with diffusion processes dictated by environmental conditions.[52, 53] A two-sample t-test was performed to compare the statistical difference between means for hGalEAm and hDMA at all three RHs (see Appendix, Table S.5). All GalEAm and DMA hydrogels containing high and low ATris loading exhibit a statistical difference between means at different RHs, with the exception of hDMA at 95% RH. High bound water GalEAm hydrogels

(h84GalEAm20BIS) exhibits lower diffusion coefficients compared to h92GalEAm20BIS (low bound water). This is also evident from simulations (see Appendix Figure A.8) where the translational mobility of the bulk water molecules slightly decreased with increased ATris in GalEAm hydrogels containing 20% BIS loading.

GalEAm and DMA hydrogels exhibit diffusion coefficients of a similar order of magnitude (Table 2.2), and according to the t-test there is no statistical difference between the means of h84DMA20BIS and h84GalEAm20BIS at 35 and 60% RH. However, the water molecules in h92GalEAm20BIS show marginally higher diffusion coefficients compared to h92DMA20BIS and are statistically different at all RHs. This might be due to the higher mobility of side chains in GalEAm systems compared to DMA gels. It has been previously shown that water molecules move concurrently with the polymer groups due to their hydrogen bonding capabilities.[41] Thus, any differences in the side chain mobility of the gels will affect the mobility of water, due to the coupled motion between water and the polymer.

2.4 Conclusions

The complex physicochemical properties associated with water-polymer and water-water hydrogen bonding dynamics within bioinspired acrylamide copolymer glycohydrogels containing stereospecific galactose pendant groups was examined. A coupled experimental and simulation approach was used to establishes a fundamental understanding of the factors that influence water mobility within glycohydrogel architectures. Furthermore, an acrylamide comonomer with a pendant siloxane group provided additional insight toward glycohydrogels containing highly hydrophobic

composition, providing a platform for the improved design of biologically relevant materials that have substantial implications in biomedical applications. In order to probe the significance of hydrogen bonding potential analogous DMA copolymer hydrogels were synthesized as a control.

Glycohydrogels provided experimentally tailorable high equilibrium water content polymer networks, where low EWC glycohydrogels exhibited a higher concentration of bound water. Although galactose groups provide ample hydrogen bonding potential, it was found that hydrophilicity alone is not sufficient to promote structural water formation. Analysis of water mobility by both simulations and DVS suggests that the environment in which confined water exists dictates the fraction of bound water within the system. Lifetime analysis of water-polymer hydrogen bonding showed a broader range with respect to EWC for glycohydrogels, with low EWC hydrogels exhibiting the longest hydrogen bonding lifetimes of ~15ps. On the other hand, DMA hydrogels did not show tunable EWC and bound water content. Overall, it was found that a balance between hydrophobic composition and crosslinker loading is necessary to disrupt water-water clustering and promote water-polymer interactions in glycohydogels.

2.5 References

1. Roger, P., et al., Effect of the incorporation of a low amount of carbohydrate-containing monomer on the swelling properties of polyacrylamide hydrogels. *Polymer* **2007,** *48* (26), 7539-7545.
2. Zhou, W.-J., et al., Synthesis and thermal properties of a novel lactose-containing poly(N-isopropylacrylamide-co-acrylamidolactamine) hydrogel. *Journal of Polymer Science Part A: Polymer Chemistry* **2000,** *37* (10), 1393-1402.
3. Müller-Plathe, F., Different States of Water in Hydrogels? *Macromolecules* **1998,** *31* (19), 6721-6723.

4. Tamai, Y., et al., Molecular Dynamics Study of Polymer−Water Interaction in Hydrogels. 1. Hydrogen-Bond Structure. *Macromolecules* **1996,** *29* (21), 6750-6760.
5. Cursaru, B., et al., *The states of water in hydrogels synthesized from diepoxy-terminated poly(ethylene glycol)s and aliphatic polyamines*. 2010; Vol. 72, p 99-114.
6. Gun'ko, M. V., et al., Properties of Water Bound in Hydrogels. *Gels* **2017,** *3* (4).
7. Mani, S., et al., Structure and Hydrogen Bonding of Water in Polyacrylate Gels: Effects of Polymer Hydrophilicity and Water Concentration. *The Journal of Physical Chemistry B* **2015,** *119* (49), 15381-15393.
8. Das, P. K., et al., Aqueous RAFT Synthesis of Glycopolymers for Determination of Saccharide Structure and Concentration Effects on Amyloid β Aggregation. *Biomacromolecules* **2017**.
9. Tranoudis, I.; Efron, N., Water properties of soft contact lens materials. *Contact Lens and Anterior Eye* **2004,** *27* (4), 193-208.
10. Ahmad, M. B.; Huglin, M. B., DSC studies on states of water in crosslinked poly(methyl methacrylate-co-n-vinyl-2-pyrrolidone) hydrogels. *Polymer International* **1994,** *33* (3), 273-277.
11. Burnett, D. J., et al., Measuring moisture sorption and diffusion kinetics on proton exchange membranes using a gravimetric vapor sorption apparatus. *Journal of Power Sources* **2006,** *160* (1), 426-430.
12. Frisch, H. L., "Diffusion in polymers" edited by J. Crank and G. S. Park, Academic Press, London and New York, 1968; 452 pg. *Journal of Applied Polymer Science* **1970,** *14* (6), 1657-1657.
13. Plimpton, S., Fast Parallel Algorithms for Short-Range Molecular Dynamics. *Journal of Computational Physics* **1995,** *117* (1), 1-19.
14. Hockney, R. W.; Eastwood, J. W., *Computer Simulation Using Particles*. Taylor and Francis: New York, 1988.
15. Parrinello, M.; Rahman, A., Polymorphic transitions in single crystals: A new molecular dynamics method. *Journal of Applied Physics* **1981,** *52* (12), 7182-7190.
16. Shinoda, W., et al., Rapid estimation of elastic constants by molecular dynamics simulation under constant stress. *Physical Review B* **2004,** *69* (13), 134103.
17. Khare, R., et al., Generation of glass structures for molecular simulations of polymers containing large monomer units: application to polystyrene. *Macromolecules* **1993,** *26* (26), 7203-7209.
18. Lin, P.-H.; Khare, R., Molecular Simulation of Cross-Linked Epoxy and Epoxy−POSS Nanocomposite. *Macromolecules* **2009,** *42* (12), 4319-4327.
19. Wang, J., et al., Automatic atom type and bond type perception in molecular mechanical calculations. *Journal of Molecular Graphics and Modelling* **2006,** *25* (2), 247-260.
20. Wang, J., et al., Development and testing of a general amber force field. *Journal of Computational Chemistry* **2004,** *25* (9), 1157-1174.
21. Berendsen, H. J. C., et al., The missing term in effective pair potentials. *The Journal of Physical Chemistry* **1987,** *91* (24), 6269-6271.
22. Ryckaert, J.-P., et al., Numerical integration of the cartesian equations of motion of a system with constraints: molecular dynamics of n-alkanes. *Journal of Computational Physics* **1977,** *23* (3), 327-341.

23. Sun, H.; Rigby, D., Polysiloxanes: ab initio force field and structural, conformational and thermophysical properties. *Spectrochimica Acta Part A: Molecular and Biomolecular Spectroscopy* **1997,** *53* (8), 1301-1323.
24. Frischknecht, A. L.; Curro, J. G., Improved United Atom Force Field for Poly(dimethylsiloxane). *Macromolecules* **2003,** *36* (6), 2122-2129.
25. Habenschuss, A., et al., Structure of Poly(dialkylsiloxane) Melts: Comparisons of Wide-Angle X-ray Scattering, Molecular Dynamics Simulations, and Integral Equation Theory. *Macromolecules* **2007,** *40* (19), 7036-7043.
26. Striolo, A., et al., Thermodynamic and Transport Properties of Polyhedral Oligomeric Sislesquioxanes in Poly(dimethylsiloxane). *The Journal of Physical Chemistry B* **2005,** *109* (30), 14300-14307.
27. Striolo, A., et al., Effective Interactions between Polyhedral Oligomeric Sislesquioxanes Dissolved in Normal Hexadecane from Molecular Simulation. *Macromolecules* **2005,** *38* (21), 8950-8959.
28. Narain, R., et al., Synthesis and characterization of polymers containing linear sugar moieties as side groups. *European Polymer Journal* **2002,** *38* (2), 273-280.
29. Yokota, M., et al., The Role of Amide Groups in Vinyl Monomers Containing Siloxane Groups for Highly Oxygen Permeable Hydrogels. *Bulletin of the Chemical Society of Japan* **2012,** *85* (5), 584-591.
30. Yokota, M., et al., *Synthesis of a Novel Silicone Monomer Bearing Amide Groups to Improve Compatibility with Hydrophilic Vinyl Monomers*. 2011; Vol. 40, p 858-859.
31. Brostow, W., et al., Prediction of glass transition temperatures: Binary blends and copolymers. *Materials Letters* **2008,** *62* (17), 3152-3155.
32. Khabaz, F.; Khare, R., Glass Transition and Molecular Mobility in Styrene–Butadiene Rubber Modified Asphalt. *The Journal of Physical Chemistry B* **2015,** *119* (44), 14261-14269.
33. Khabaz, F., et al., Temperature Dependence of Volumetric and Dynamic Properties of Imidazolium-Based Ionic Liquids. *The Journal of Physical Chemistry B* **2018,** *122* (8), 2414-2424.
34. Soldera, A.; Metatla, N., *Glass transition of polymers: Atomistic simulation versus experiments*. 2007; Vol. 74, p 061803.
35. Soni, N. J., et al., Effect of cross-linker length on the thermal and volumetric properties of cross-linked epoxy networks: A molecular simulation study. *Polymer* **2012,** *53* (4), 1015-1019.
36. Silva, M. E. S. R. e., et al., Preparation and thermal study of polymers derived from acrylamide. *Polymer Degradation and Stability* **2000,** *67* (3), 491-495.
37. Yokota, M., et al., Novel Method for Surface Modification of Silicone-containing Hydrogel Using Addition Reaction. *Chemistry Letters* **2011,** *40* (11), 1297-1299.
38. Ikeda-Fukazawa, T., et al., Effects of crosslinker density on the polymer network structure in poly-N,N-dimethylacrylamide hydrogels. *Journal of Polymer Science Part B: Polymer Physics* **2013,** *51* (13), 1017-1027.
39. Orakdogen, N., et al., Suppression of inhomogeneities in hydrogels formed by free-radical crosslinking copolymerization. *Polymer* **2005,** *46* (25), 11407-11415.

40. Urata, S., et al., Molecular Dynamics Simulation of Swollen Membrane of Perfluorinated Ionomer. *The Journal of Physical Chemistry B* **2005,** *109* (9), 4269-4278.
41. Khabaz, F., et al., Molecular Origins of Dynamic Coupling between Water and Hydrated Polyacrylate Gels. *Macromolecules* **2016,** *49* (19), 7551-7562.
42. Balasubramanian, S.; Bagchi, B., Slow Orientational Dynamics of Water Molecules at a Micellar Surface. *The Journal of Physical Chemistry B* **2002,** *106* (14), 3668-3672.
43. Laage, D.; Hynes, J. T., A Molecular Jump Mechanism of Water Reorientation. *Science* **2006,** *311* (5762), 832-835.
44. Laage, D., et al., Why Water Reorientation Slows without Iceberg Formation around Hydrophobic Solutes. *The Journal of Physical Chemistry B* **2009,** *113* (8), 2428-2435.
45. Luzar, A.; Chandler, D., Structure and hydrogen bond dynamics of water–dimethyl sulfoxide mixtures by computer simulations. *The Journal of Chemical Physics* **1993,** *98* (10), 8160-8173.
46. Luzar, A.; Chandler, D., Effect of Environment on Hydrogen Bond Dynamics in Liquid Water. *Physical Review Letters* **1996,** *76* (6), 928-931.
47. Larson, R. G., *The structure and rheology of complex fluids*. New York (N.Y.) : Oxford university press: 1999.
48. Grdadolnik, J., et al., Origin of hydrophobicity and enhanced water hydrogen bond strength near purely hydrophobic solutes. *Proceedings of the National Academy of Sciences* **2016**.
49. Godawat, R., et al., Characterizing hydrophobicity of interfaces by using cavity formation, solute binding, and water correlations. *Proceedings of the National Academy of Sciences* **2009,** *106* (36), 15119.
50. Remsing, R. C., et al., Pathways to dewetting in hydrophobic confinement. *Proceedings of the National Academy of Sciences* **2015,** *112* (27), 8181.
51. Weinmüller, C., et al., Sorption kinetics and equilibrium uptake for water vapor in soft-contact-lens hydrogels. *Journal of Biomedical Materials Research Part A* **2006,** *77A* (2), 230-241.
52. Ahmed, E. M., Hydrogel: Preparation, characterization, and applications: A review. *Journal of Advanced Research* **2015,** *6* (2), 105-121.
53. Jones, L., et al., In vitro evaluation of the dehydration characteristics of silicone hydrogel and conventional hydrogel contact lens materials. *Contact Lens and Anterior Eye* **2002,** *25* (3), 147-156.

CHAPTER III – Viscoelastic Properties of Glycohydrogels During and Post Gelation, Measured via Rheology

3.1 Introduction

Evaluating the elastic properties of glycohydrogels as a function of network composition, crosslink density, and the swelling environment is important for understanding the mechanical properties and network stability which dictate the overall handleability of bulk hydrogels as well as their suitable applications. Due to the inherent hydrophilicity of saccharides, glycohydrogels are high water content hydrogel materials. Despite the high potential for water-polymer hydrogen bonding modes, we found that hydrophobicity is an important structural component to facilitate confined water levels, and hydrophobic comonomers can be used in hydrogel architectures to tune equilibrium water content. Depending on the nature of the hydrophobic component and the method of copolymerization, mechanical properties and molecular architecture are also modulated.[1] Measuring the viscoelastic properties of hydrogels via rheometry provides valuable insight toward hydrogel network architecture (e.g., molecular weight between crosslinks), modes of relaxation, mechanical strength, and dimensional network stability.

The majority of research that examines the mechanical properties of complex glycohydrogels is targeted toward responsive delivery systems, where copolymers are often comprised of pH or thermally responsive constituents.[2-4] By utilizing polymers with pendant saccharide moieties (e.g., galactose, glucose, or sucrose), targeted material delivery is assisted due to favorable binding interactions at the cell surface. Typically, responsive comonomers such as N-isopropyl acrylamide (NIPAM) are utilized,[5, 6] which can be hydrophilic depending on the conditions of the swelling environment. Therefore,

relevant literature is focused on diffusional and elastic properties of glycohydrogels dictated by physical changes to the polymer network as a response to an external stimulus. Although extensive research has been published on the properties of common hydrogel architectures (such as HEMA) that have been hydrophobically modified,[7, 8] limited information exists for the effects of hydrophobicity in glycohydrogels on mechanical properties. Specifically, contributions to the fundamental understanding of the effects of amphipathic balance and crosslinking density on the viscoelastic properties of covalently crosslinked glycopolymer hydrogels properties will allow for better physical design of biologically compatible materials.

Rheological monitoring of polymerization kinetics in situ provides additional information about the viscoelastic transition from a low viscosity reactive mixture (sol) to a soft solid-like hydrogel material (gel). This provides a valuable understanding of both the effects of reactive solution composition (e.g., monomer/crosslinker identity and concentration) and polymerization parameters (e.g., temperature and solvent type) on elastic properties of crosslinked hydrogels. Furthermore, polymerizing hydrogels directly between the selected geometry has the additional advantage of preventing sample slippage at the material/plate geometry surface during oscillatory tests. Sample slippage is a common issue for rheological measurements of pre-gelled and highly swollen soft materials. Subsequent rheological tests such as strain (τ) and frequency (ω) sweeps can be immediately performed to measure linear viscoelastic regime (LVR), complex viscosity (η^*), and complex shear modulus (G^*) of hydrogels in situ. Equation 3.1 and Equation 3.2 define G^* and η^* where G' is the elastic component (storage modulus) and G" is the viscous component responsible for energy lost during flow (loss modulus).

$G^* = G' + iG''$ ..... Equation 3.1

$\eta^* = \eta' - i\eta'' = G'/\omega - iG''/\omega$ ..... Equation 3.2

In this study, copolymer GalEAm and DMA hydrogels containing 10 mol% BIS loading examined in Chapter II were analyzed via rheology to determine their viscoelastic properties. Additionally, a series of GalEAm and DMA homopolymer hydrogels with varying BIS loading were examined to: (1) establish a baseline for comparison to copolymer hydrogels and (2) to further understand the effects of effective crosslink density on glycopolymer hydrogels. The rheological monitoring method was used to prepare the hydrogels directly between the parallel plate geometries using UV-initiated free radical polymerization. Subsequent rheological tests were performed on hydrogels in situ providing insight toward the mechanical properties and network architecture of select hydrogels which were extensively studied for their hydration characteristics.

3.2 Experimental

3.2.1 Hydrogel design and preparation

All homopolymer and copolymer reactive formulations were prepared and purged with ultra-high purity nitrogen immediately before rheological measurements in a UV-light filtered environment. DMA and GalEAm homopolymer hydrogels containing four BIS loadings (5, 8, 10, and 15 mol%) were prepared in DMSO using the stock solution method discussed in Chapter 2.2.3.2. A similar naming strategy was used where the percent monomer and crosslinker are defined (e.g., h100DMA5BIS contains only DMA as the monomer and 5 mol% BIS loading). The UV initiator concentration (Irgacure 2959) and monomer concentration were kept constant at 0.05 mol% and 1M. Copolymer

hydrogels with 10 mol% BIS were prepared using an additional stock solution containing ATris and the same naming strategy discussed in Chapter 2.2.3.2 was used.

3.2.2 Rheology testing methods

Viscoelastic properties of hydrogels during and post gelation were performed using a TA Instruments stress-controlled ARES rheometer equipped with a Waveform and Fast Data Sampling option (National Instruments DAQ-Pad) and UV-cure accessory. All tests were conducted at room temperature and performed in triplicate using 20mm parallel plates (acrylic top and aluminum bottom), 0.5 mm gap height, and a frequency of 1 rad/s. Dynamic time sweeps were conducted to monitor the change in viscoelastic properties during polymerization of hydrogel formulations upon exposure to UV-light (10 ± 2 mW/cm2) using an Omnicure 2000 (200 W lamp) light source. Although a high strain is needed to generate suitable torque values for low viscosity materials (such as the reactive formulations before gelation), a significant increase in modulus after gelation occurs requiring low strain. Automatic tension and strain adjustment testing options are available for the ARES rheometer but enabling this function for the fast data sampling option will cause discontinuities in the data.[9] Therefore, a low strain of 1% was chosen for all hydrogel systems examined to stay within the motor and transducer limitations of the rheometer as well as the linear viscoelastic regime. Measurements were taken every 500ms with a correlation cycle of 1 resulting in a high data acquisition rate of 3.5 pts/cycle. The test was stopped, and the normal force zeroed upon achieving the plateau modulus. Dynamic time sweep data was analyzed using the OriginLab® software. Immediately following the time sweep, a dynamic frequency sweep from 0.1 to 100 rad/s, in both the up and down direction, was performed using a 1% strain rate. The linear

viscoelastic regime of crosslinked hydrogels was determined by performing strain sweeps between 0.1 to 50% strain at 1 rad/s.

3.2.3 Calculation of fit parameters for time sweep profiles

Periodic cycling affected the measured storage modulus at the end of the sol/gel process in all measurements. Therefore a smoothing function was applied to the measured storage modulus data using a percentile filter method with a 15-point window. The Hill fitting function was then implemented using a Levenberg Marquardt iteration algorithm to generate the fit parameters and evaluate the goodness of fit.[1, 10] The time-dependent properties of the elastic modulus during polymerization was analyzed using a modified Hill equation (Equation 3.3) where θ is the time to half-gelation ($G_p'/2$) and *n* is a coefficient related to the asymptotic slope at θ.

$$G'(t) = G_p' \frac{t^n}{t^n + \theta^n} \quad \text{Equation 3.3}$$

The origins of the Hill model are from pharmacological applications where the calculated parameters represent the concentration effects of hemoglobin dissociation in solution.[11] The model has been widely adopted and modified to allow for quantitative analysis of the rate at which elastically effective crosslinks form during the sol/gel transition using Equation 3.4, where *n* is calculated using the asymptotic slope at time θ (P_θ).[1, 12, 13]

$$P_\theta = \frac{nG_p'}{4\theta} \quad \text{Equation 3.4}$$

3.3 Results and Discussion

3.3.1 Description and analysis of the viscoelastic properties during polymerization

In general, all reactive hydrogel mixtures exhibit three distinct stages defined by the evolution of viscoelastic properties during polymerization (illustrated in Figure 3.1). First, there is an induction period where the reactive formulation is exposed to UV-light, and the reactive components begin to polymerize, forming oligomers and short chain polymers. Molecular weight increases during the induction period, but G' and G" are negligible due to the low initial viscosity of the reactive mixture. The second stage is referred to as the sol/gel transition and begins when the reactive formulation transitions from a low viscosity liquid (sol) to a soft solid with a measurable modulus (gel). As the polymerization progresses, G'(t) increases monotonically until it reaches an equilibrium resulting in the plateau modulus (G'_p) regime. At this stage, the hydrogel is considered fully crosslinked and G' dominates the viscoelastic response.

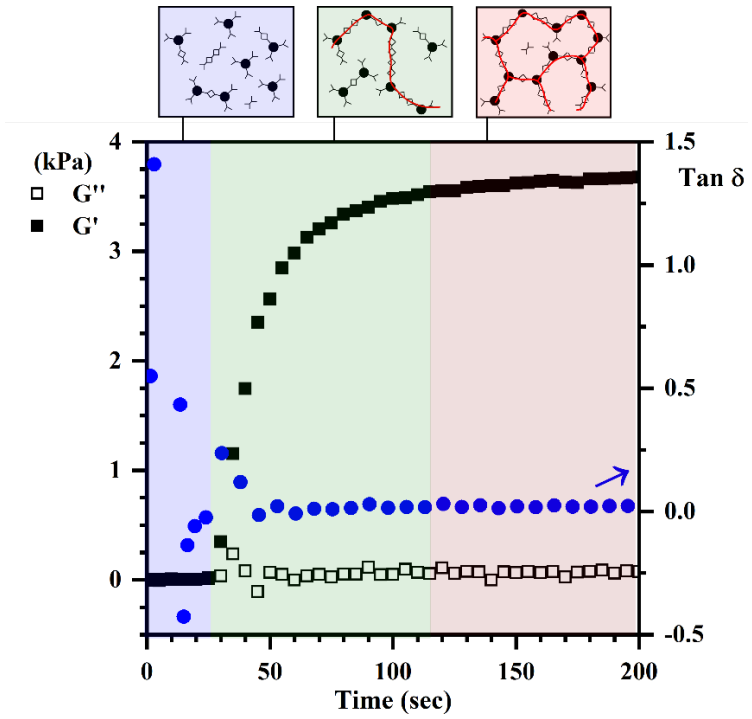

Figure 3.1 Illustration of the induction (blue), sol/gel transition (green), and plateau modulus (pink) regimes associated with the change in viscoelastic properties measured during the polymerization of 100GalEAm5BIS using a rheological time sweep test performed at a constant strain and frequency.

Monitoring the UV initiated polymerization via rheology is challenging due to the fast gelation kinetics, change in moduli over 2-4 orders of magnitude, and dimensional changes of the system. Shown in Figure 3.2 is an example of a typical rheokinetic curve collected using the ARES fast data sampling option, where the change in viscoelastic properties (sol/gel transition) during polymerization of h100GalEAm8BIS was monitored in situ. Most of the homopolymer and copolymer hydrogels examined exhibited periodic cycling of G' as G'(t) approached G_p', an example is shown in Figure 3.2.a. Common stress- or strain-controlled rheometers acquire dynamic mechanical data using data

acquisition and correlation systems that have limited data sampling capability.[14] The ARES fast data sampling option significantly enhances the rheokinetic resolution of the sol/gel transition behavior by improving the data correlation speed and sensitivity.[15] The enhanced sensitivity is a result of the improved signal to noise ratio, where the noise is the uncertainty of the measured modulus and phase.[15, 16] Although the improved torque sensitivity and high rate of data collection allowed for the analysis of the sol/gel transition kinetics, it is also responsible for the periodic cycling at G'_p. The large increase in modulus and inability to modulate strain during full gelation coupled with enhanced torque sensitivity resulted in periodic cycling concurrent with the defined frequency of 1 rad/s. Although this effect is in response to a material property, the symmetric behavior and alignment with testing cycles suggests that it is purely an instrumental artifact. Therefore, as shown in Figure 3.1.b, a smoothing function was used to remove the symmetric periodic noise in the data, and the G'(t) profile was fit using the modified Hill equation (red line). The embedded table contains an example of the generated fit parameters and indices to determine the goodness of fit. All measured samples that exhibited this behavior were treated with the same smoothing method, and Hill fit analysis, where an adjusted-R^2 value close to one was achieved.

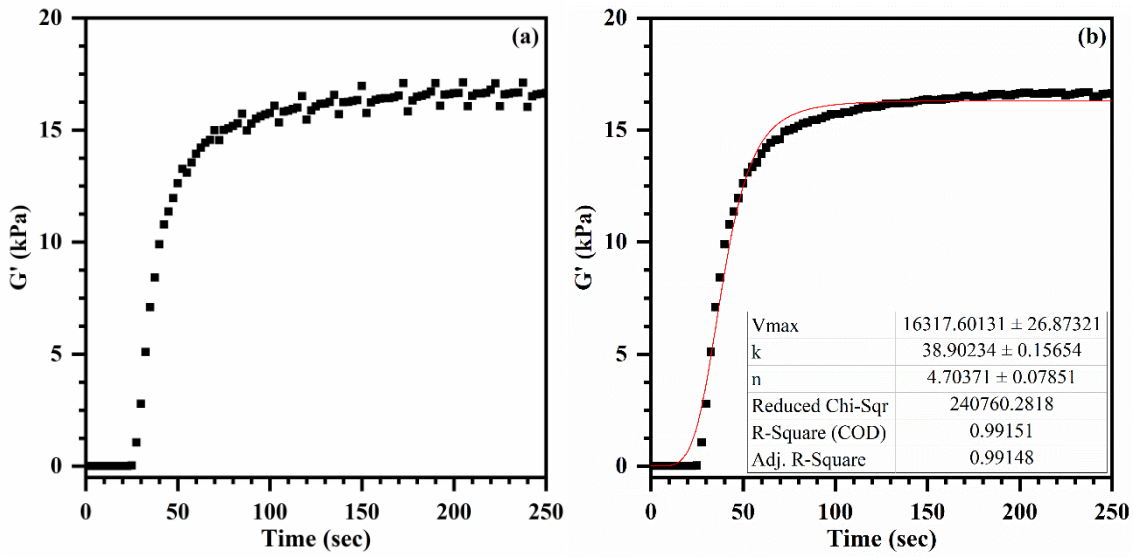

Figure 3.2 (a) Example of a G'(t) profile generated during polymerization of h100GalEAm8BIS exhibiting periodic noise in the data observed during the final stages of polymerization. (b) Results of smoothing the G'(t) data and Hill fit summary (red line).

3.3.2 Rheokinetics of GalEAm and DMA homopolymer hydrogels

The rheokinetic profiles for h100GalEAm and h100DMA hydrogels with varying crosslinker concentration are shown in Figure 3.3. A typical viscoelastic response is observed where G' is orders of magnitude greater than G". As expected, an increase in G'_p is observed with respect to higher BIS loading for both GalEAm and DMA hydrogels. Although the G" at full gelation is insignificant compared to G'_p, there is a slight increase in G" with respect to BIS loading both for the h100GalEAm and h100DMA hydrogels. Trends in the G' and G" modulus at full gelation as a function of crosslinker concentration are described in detail in the following section. Differences in the rheokinetic behavior between GalEAm and DMA hydrogels are reflected in the sigmoidal shape of the storage modulus shown in Figure 3.3.a & b. For h100DMA, the

induction period and sol/gel duration are highly dependent on the BIS loading, where the sigmoidal shape is elongated at low %BIS. Whereas for h100GalEAm the sigmoidal shape is unchanged in terms of the induction and sol/gel duration across all BIS loadings with a much larger range in the magnitude of G'_p.

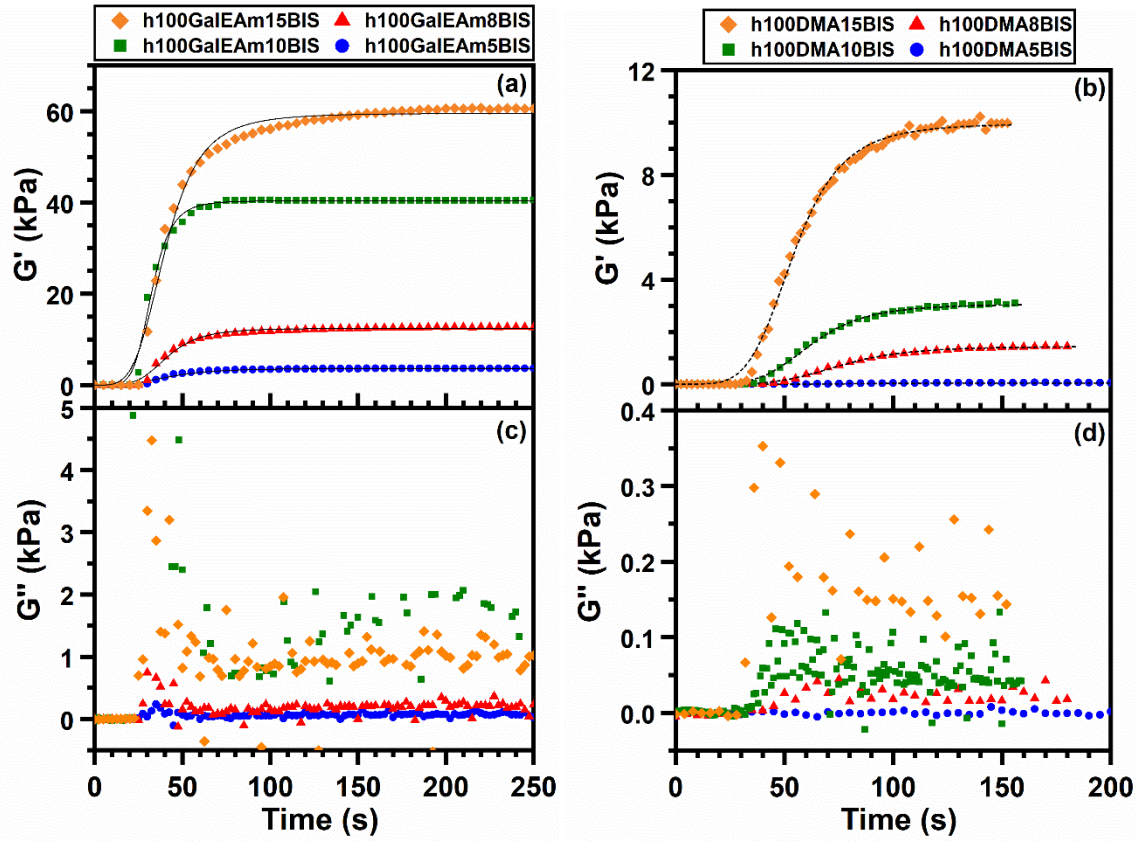

Figure 3.3 Change in the elastic (a,b) and viscous (c,d) modulus for h100GalEAm (left) and h100DMA (right) hydrogels during polymerization of reactive mixtures containing varying amount of BIS loading (dotted line in G'(t) is the predicted fit from the Hill equation analysis). Both systems exhibit an increase in G'_p with an increase in BIS loading.

The generated fit parameters, summarized in Figure 3.4, allow for quantitative analysis of trends observed in the rheokinetic profiles. Regardless of BIS loading, the time to half-gelation remains unchanged for h100GalEAm hydrogels ($\theta \approx 40$ sec). Whereas θ for the h100DMA initially decreases from 85 to 78 sec for hydrogels with less than10 mol% BIS and levels out above10 mol% BIS. The differences observed between θ_{DMA} and θ_{GalEAm} are most likely associated with the monomer mobility during polymerization. Mobility of GalEAm is hindered by the steric bulk of the pendant saccharide unit and high propensity to form inter/intra molecular hydrogen bonds through the abundant free hydroxyl groups. Linear glycopolymers have been shown to aggregate in solution due to cooperative inter/intra molecular hydrogen bonding between hydroxyl groups on the saccharide unit.[17, 18] Furthermore, formation of non-permanent crosslinks through hydrogen bonding can contribute to the elastic modulus.[12] As the molecular weight of the polymer segments begins to grow and covalent crosslinks are formed, the GalEAm-OH groups begin to participate in inter/intra molecular hydrogen bonding (illustrated in Scheme 3.1). The storage modulus rapidly increases during the sol/gel transition due to the quick formation of hydrogen bonded GalEAm clusters, overshadowing any potential effects of BIS loading on gelation kinetics. On the other hand, DMA does not undergo hydrogen bonding and is significantly less sterically hindered allowing for greater mobility. Therefore, it is reasonable that differences in θ for h100DMA below a certain threshold of BIS loading is observed. Similar reasoning can be applied to the differences in the magnitude of G'_p as BIS loading is increased (shown in Figure 3.4.b); G'_p for h100GalEAm increases by about six orders of magnitude whereas G'_p for h100DMA only increases by one order of magnitude.

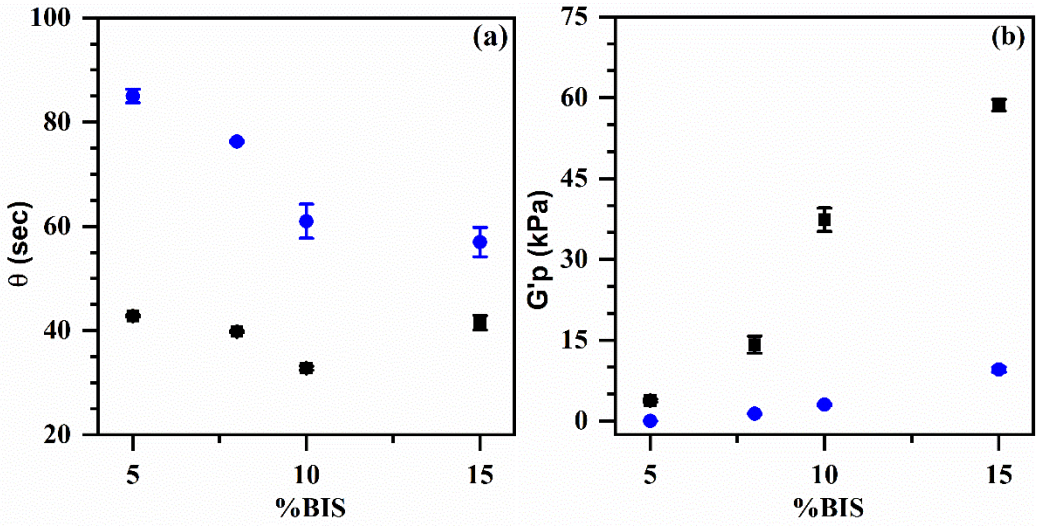

Figure 3.4 The (a) time to half-gelation (θ) and (b) G_p' for h100GalEAm (black square) and h100DMA (blue circle). For h100GalEAm θ remains unchanged while G_p' changes with respect to BIS loading, this is a result of inter/intra molecular hydrogen bonding and steric bulk. DMA mobility is uninhibited by physical interactions resulting in softer hydrogels where θ is modulated by BIS loading.

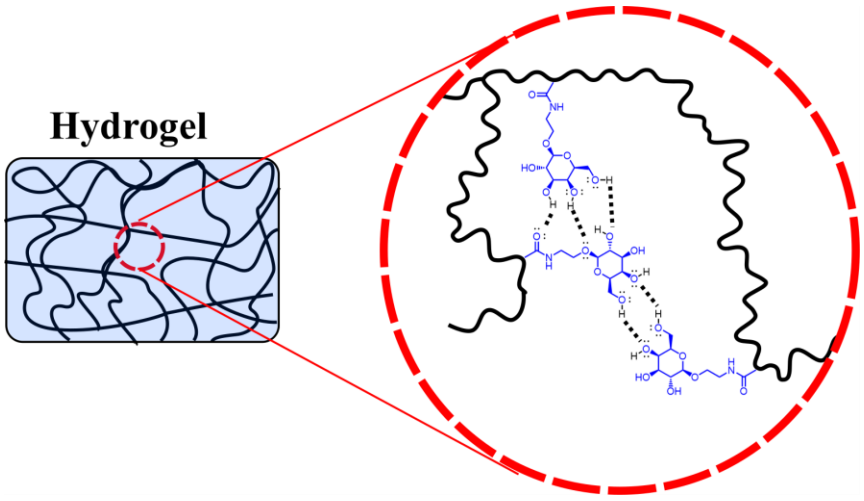

Scheme 3.1 Illustration of hydrogen bonded clusters formed between pendant galactose units during the polymerization of h100GalEAm hydrogels.

3.3.3 Influence of BIS loading on viscoelastic properties of GalEAm and DMA homopolymer hydrogels

The effect of increasing frequency on the average G' and G" modulus is shown in Figure 3.5. Complete polymerization was verified by the reproducibility of G'(ω) performed between 0.1 and 100 rad s^{-1} in the up and down direction (decreasing frequency measurements are shown in Appendix Figure B.1). The stability and dominant elastic behavior (G'>>G") of G'(t) across all BIS loadings for h100GalEAm and h100DMA hydrogels indicates the formation of an elastically effective crosslinked network. Furthermore, the storage modulus measured as a function of frequency is in good agreement with G_p'. As observed in the rheokinetic profiles, the DMA hydrogels are significantly softer than the GalEAm hydrogels (the average G' shown in Figure 3.5.a&c legend). The increase in the average G"(ω) at high BIS loading for both DMA and GalEAm is attributed to an increase in trapped solvent viscosity.[12] Differences between h100DMA and h100GalEAm in G"(ω) were observed. For h100DMA, G" remained unchanged at all levels of BIS loading (Figure 3.4.d). The large G" error associated with h100DMA5BIS is a result of the formation of a soft gel (G' ~ 20Pa) resulting in a high signal to noise ratio. This was the only sample that did not retain its physical shape upon removal from the testing fixture. On the other hand, G" of h100GalEAm hydrogels at the low and high levels of BIS loading exhibited frequency dependent behavior, where G" slightly increases with increasing frequency. At high ω, relaxation mechanisms occur at a shorter time scale and are generally a result of local relaxations. The viscous modulus is affected by the captured solvent viscosity and potential formations of network inhomogeneities (e.g., free dangling chain end, crosslinker aggregation, and physical

entanglements).[12, 19] This supports the claim that inter/intra molecular hydrogen bonding is occurring within h100GalEAm hydrogels, resulting in an increase in effective solution viscosity.

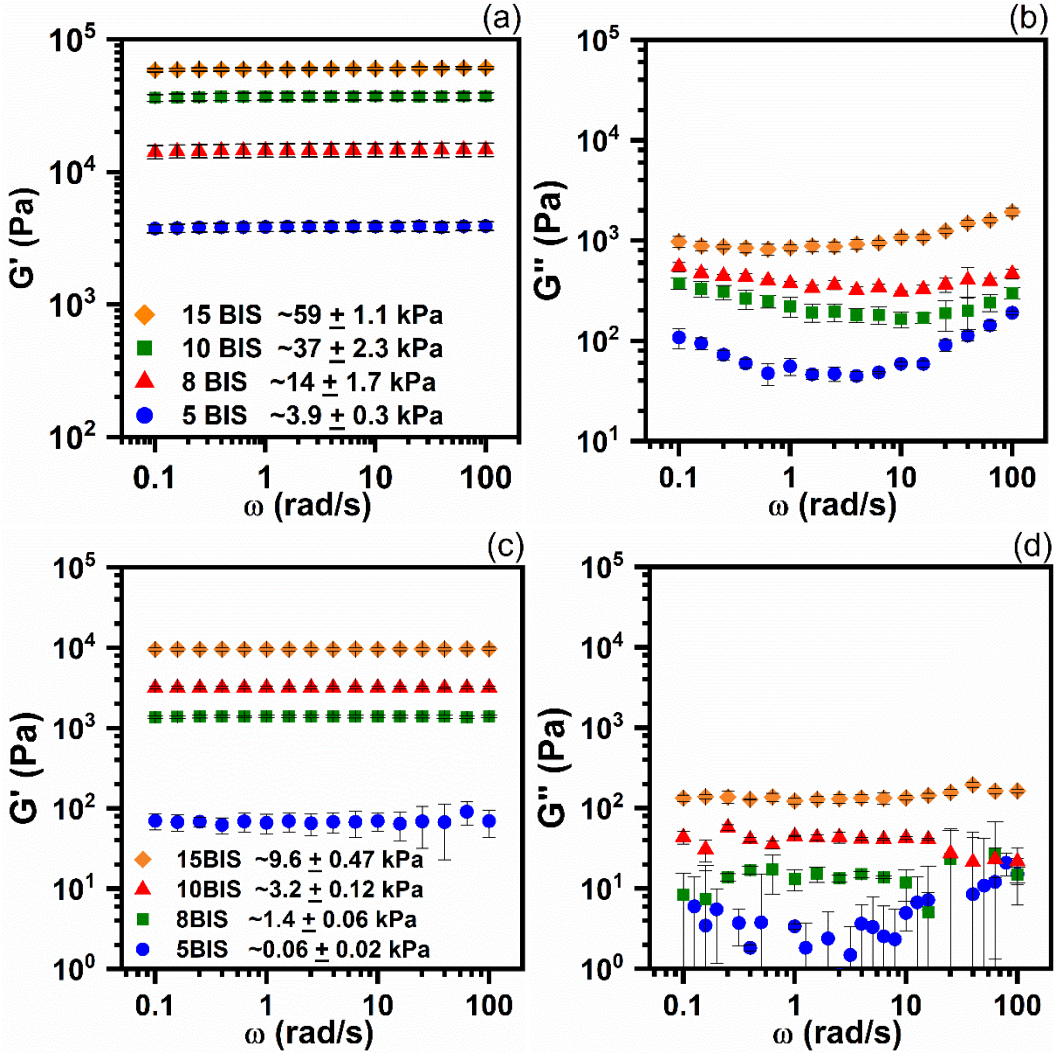

Figure 3.5 The average storage (a,c) and loss (b,d) modulus of h100GalEAm (top) and h100DMA (bottom) with varying BIS loading as a function of frequency (ω) ramped from 0.1 to 100 rad/s. The average G' and standard deviation is embedded in the figure legend.

Tan δ (calculated by G”/G’) as a function of frequency is shown in Figure 3.6. Tan δ is a measure of the system’s ability to dissipate energy. Since G’ remained constant with respect to ω changes in Tan δ are caused by G”. For h100DMA, tan δ remains constant with respect to frequency. Large variation in low BIS loading is attributed to the soft, gel-like properties shown previously. Tan δ can be used to describe the mechanical nature of a hydrogel, where tan $\delta < 0.1$ are considered strong gels.[10] However, for GalEAm hydrogels the increase in G” at high frequencies results in an increase in Tan δ for low and high BIS loading. This is attributed to an increase in trapped solvent viscosity caused by the longer relaxation times of the polymer chains, which depend on non-covalent interactions (i.e., inter/intra molecular hydrogen bonding events) and molecular weight between crosslinks.[20] At low BIS loading, crosslinked GalEAm clusters have more physical freedom to form inter/intra molecular hydrogen bonds. Hydrogen bonding interactions at low BIS loading and limited flexibility of polymer chains at high crosslink density increase entrapped solution viscosity resulting in an increase in G” and tan δ at high frequencies.

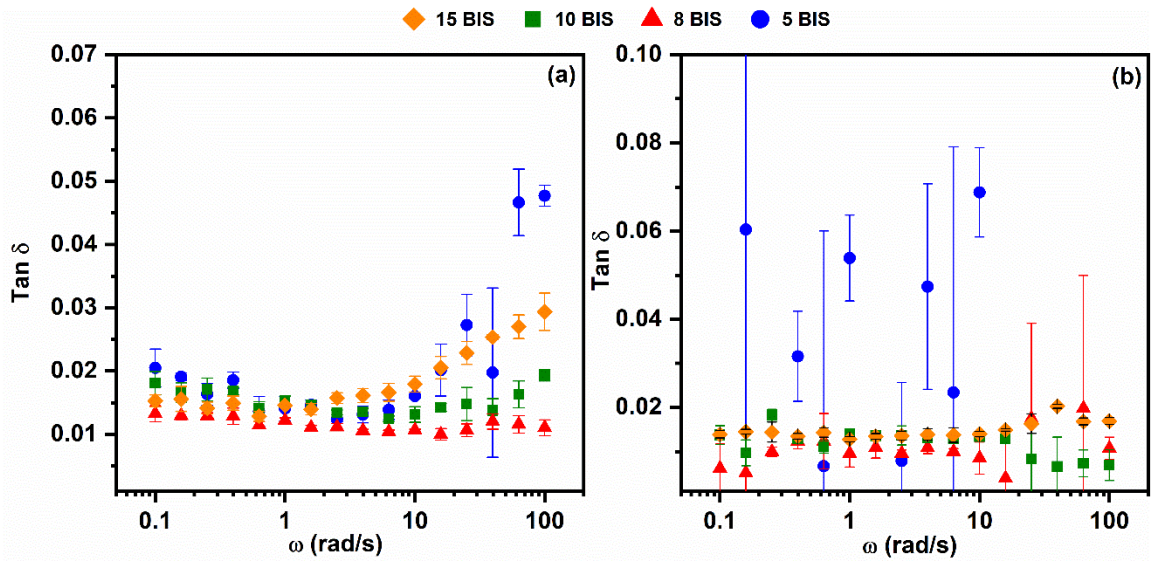

Figure 3.6 Tan δ for (a) h100GalEAm with varying BIS loading increases at high frequencies, whereas (b) h100DMA was unchanged with all BIS loading levels within experimental error.

3.3.4 Selection of hydrophobically hydrogels for rheological analysis and description of limited miscibility in GalEAm copolymer hydrogels

Copolymer composition can affect sol/gel kinetics as well as the macromolecular structure of the polymer network.[7] Due to the high rate of gelation for h100DMA and the significant increase in material modulus for h100GalEAm at high BIS loading a moderate level of BIS loading (10 mol%) was utilized to probe the effects of amphipathic balance on the viscoelastic properties. Miscibility between the GalEAm and ATris, shown in Figure 3.7, exhibits a time and concentration dependent behavior for the GalEAm copolymer hydrogels. Similar to the behavior described in Chapter 2.3.2, visible phase separation in the form of small opaque regions occurred. However, the molded hydrogels discussed in Chapter 2 were synthesized immediately after mixing the comonomers and

crosslinker by dispensing the reaction mixture into three quartz molds and simultaneously exposing them to UV light. Therefore, the phase separation observed was minimal, whereas reactive mixtures used for rheological analysis were held for long periods of time between multiple lengthy rheological tests. In order to mitigate the effect of ATris phase separation, reactive mixtures were vortexed immediately before removing an aliquot for testing. This resulted in less variation between rheological tests and visual appearance of the resulting hydrogels.

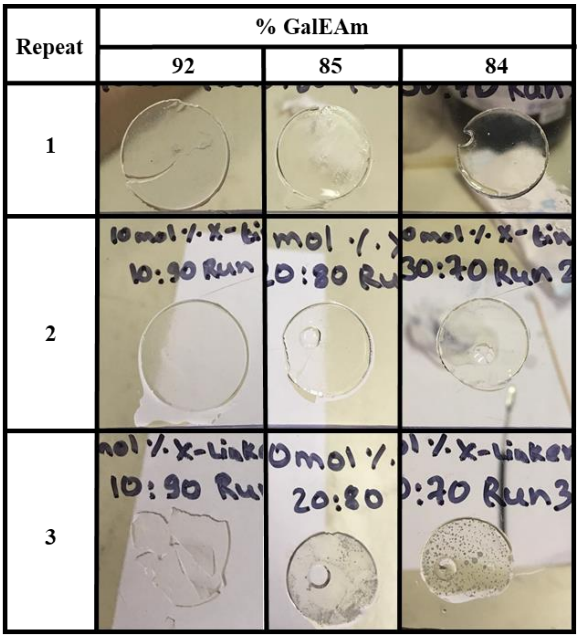

Figure 3.7 Visual properties of copolymer GalEAm hydrogels with 10 mol% BIS loading measured using in-situ UV rheology. At high ATris loading an increase in phase separation is apparent, resulting in the formation of opaque regions.

3.3.5 Rheokinetics for hydrophobically modified GalEAm and DMA comopolymer hydrogels

Comonomer incorporation of ATris into GalEAm and DMA hydrogels containing 10% BIS loading, shown in Figure 3.8, drastically lowered the elastic properties at the end of gelation resulting in a significantly softer hydrogel. The viscous modulus is negligible in comparison to G'; therefore, it can be neglected (G" shown in Appendix Figure B.2). Shown in Figure 3.9 are the rheokinetic parameters associated with the polymerization kinetics. Overall, G_p' was significantly lower in the copolymer hydrogels than in the equivalent homopolymer hydrogels. With increased loading of ATris, G_p' decreased for both hGalEAm10BIS and hDMA10BIS copolymer hydrogels. Decreased G_p' could be a result of the enhanced chain flexibility of the siloxane pendent group and formation of hydrophobic/hydrophilic clusters. ATris loading also affected the time to half gelation (Figure 3.9.a) where a longer time to θ was observed for GalEAm and DMA hydrogels containing ATris loading > 8% as compared to homopolymer hydrogels. The change in θ from low to high ATris loading in DMA (Δ 25 sec) hydrogels was greater than in GalEAm (Δ 13 sec).

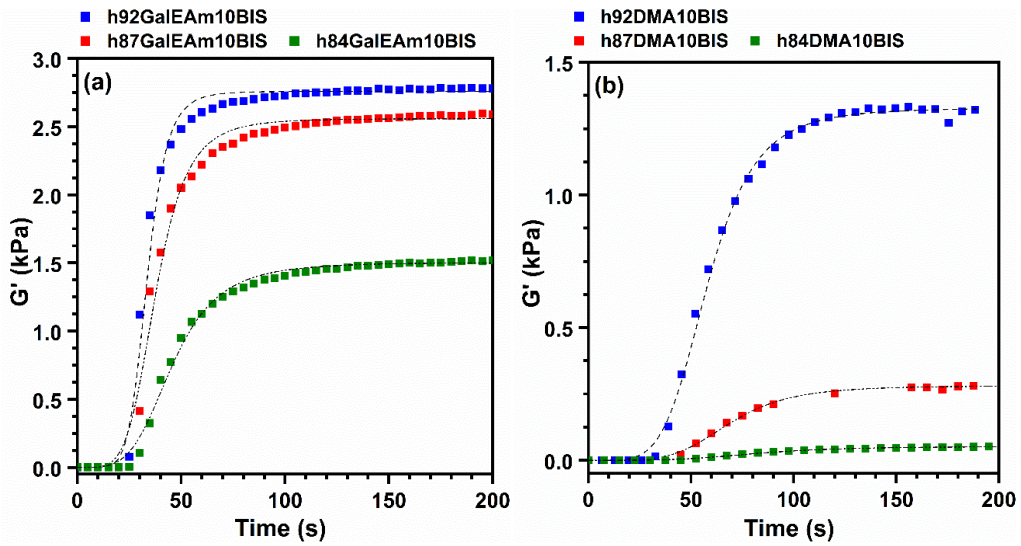

Figure 3.8 Effect of ATris loading on G' for (a) hGalEAm10BIS and (b) hDMA10BIS copolymer hydrogels during polymerization of reactive mixtures (dotted line in G'(t) is the predicted fit from the Hill equation analysis).

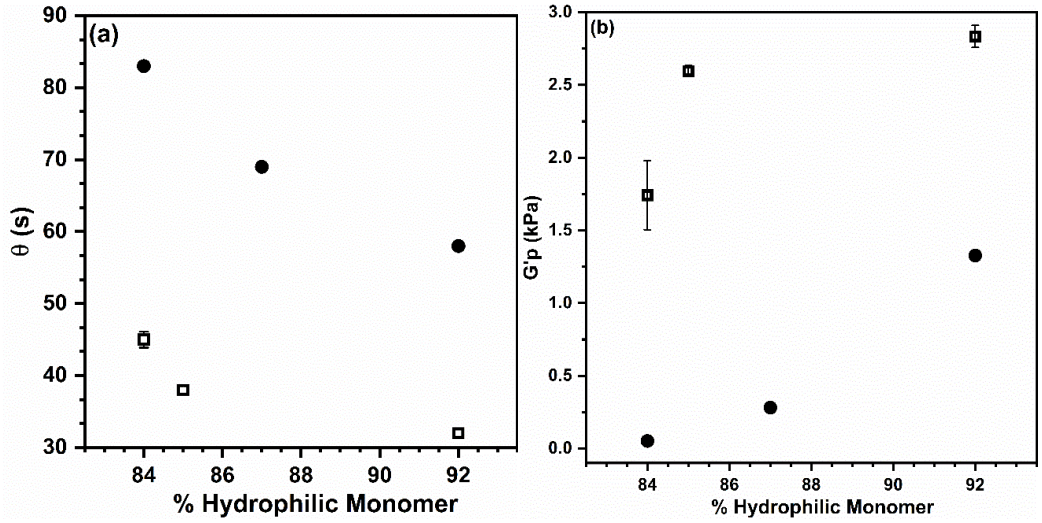

Figure 3.9 Modeled Hill fit parameters of the (a) time to half-gelation (θ) and (b) G'_p for hGalEAm10BIS (open square) and hDMA10BIS (solid circle) copolymer hydrogels. In comparison to homopolymer equivalent networks, inclusion of ATris decreased G'_p and increased θ.

3.3.6 Influences of ATris loading on viscoelastic properties of copolymer hydrogels at gelation

As expected, hydrophobic monomer inclusion in GalEAm and DMA copolymer hydrogels containing 10 mol% BIS reduced the network modulus, shown in Figure 3.10. The overall reduction of modulus is attributed to the flexibility of the pendant siloxane groups. However, the effect of ATris on the viscoelastic characteristics for GalEAm and DMA differ significantly both with respect to the reduction of G' and the frequency dependent behavior. For GalEAm copolymer hydrogels, G' remains constant and is an order of magnitude greater than G", suggesting the formation of elastically effective crosslinks. Although an increase in ATris loading for hGalEAm10BIS only slightly reduced G' (3010 to 1779 Pa), the frequency dependent behavior of G", observed in the homopolymer GalEAm hydrogel, was eliminated. This is attributed to the disruption of inter/intra molecular hydrogen bonding events between pendant galactose groups which were shown to increase the effective solution viscosity.[20] On the other hand, for hDMA10BIS, an increase in ATris loading resulted in a lower G' (1436 to 72 Pa) and an increase in frequency dependent behavior. Above 8 mol% ATris, G" for DMA10BIS exhibited a strong frequency-dependence, where G" increased with respect to frequency. This suggests a critical hydrophobic composition window for DMA hydrogels between 8 and 13% ATris which results in the formation of clustered hydrophobic regions and inhomogeneities. This is consistent with the explanation for the increase in opacity above 8% ATris reported in Chapter 2.3.2. Similar viscoelastic properties were reported for hydrophobically modified polyacrylamide hydrogels, where increased G" is attributed to disassociation of hydrophobic domains with respect to increasing frequency.[21]

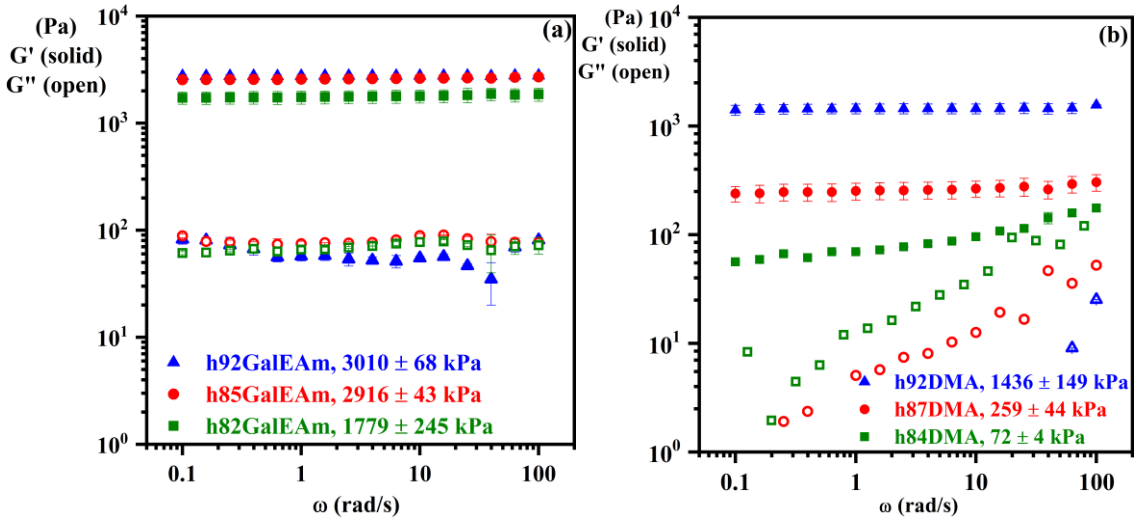

Figure 3.10 Average G' (solid) and G" (open) modulus for (a) GalEAm and (b) DMA copolymer hydrogels containing 10 mol% BIS and varying ATris loading as a function of frequency (ω) ramped from 0.1 to 100 rad/s. The average G' and standard deviation is embedded in the figure legend.

Shown in Figure 3.11, tan δ captures the differences in viscoelastic properties between hGalEAm10BIS and hDMA10BIS copolymer hydrogels. The effect of frequency on tan δ reflects the characteristics described for G' and G" in the DMA and GalEAm copolymer hydrogels. For hDMA10BIS with ATris loading greater than 8%, tan δ quickly becomes greater than 0.1 which is indicative of a weakly formed gel.[22] Furthermore, for h84DMA10BIS tan δ approached 1, suggesting that high incorporation of ATris may result in a macromolecular network structure plagued by the formation of network inhomogeneities potentially attributed to incomplete crosslinking, and the formation of loops, dangling chain ends, and hydrophobic domains.

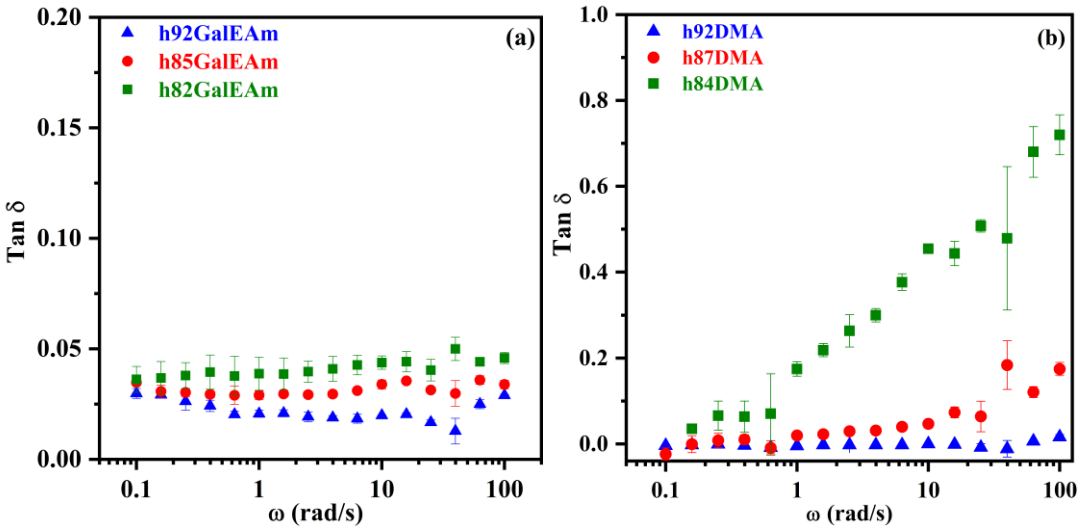

Figure 3.11 Tan δ for copolymer hydrogels where (a) hGalEAm10BIS exhibited no frequency dependency, suggesting the disruption of inter/intra molecular hydrogen bonds. At high ATris loading in (b) hDMA10BIS a significant increase in tan δ indicates the formation of network inhomogeneities.

3.4 Conclusions

The effect of macromolecular structure on the viscoelastic properties of select glycohydrogels examined in Chapter 2 were analyzed using in-situ rheology where the polymerization kinetics and viscoelastic properties provided valuable insight about the network structure. Galactose containing acrylamide homopolymer hydrogels with varying BIS loading were examined in order to understand the effects of crosslink density on polymerization kinetics and modulus in simple saccharide containing network structures. The effect of hydrophobic comonomer composition on rheokinetic behavior and viscoelastic characteristics were examined in select glycohydrogels. It was found that non-covalent interactions (e.g., inter/intra molecular hydrogen bonding) occurred within homopolymer GalEAm hydrogels. Inclusion of a hydrophobic comonomer (ATris)

disrupted the formation of non-covalent interactions. This is consistent with structural water formation within glycohydrogel structures examined in Chapter 2, where high hydrophobic loading resulted in a higher concentration of bound water content. Analogous DMA homopolymer and copolymer hydrogels were synthesized as a reference system.

3.5 References

1. Adibnia, V.; Hill, R. J., Universal aspects of hydrogel gelation kinetics, percolation and viscoelasticity from PA-hydrogel rheology. *Journal of Rheology* **2016,** *60* (4), 541-548.
2. Duan, C., et al., Galactose-decorated pH-responsive nanogels for hepatoma-targeted delivery of oridonin. (1526-4602 (Electronic)).
3. Lou, S.-F., et al., Galactose functionalized injectable thermoresponsive microgels for sustained protein release. *Colloids and Surfaces B: Biointerfaces* **2014,** *113*, 368-374.
4. Burek, M., et al., Thermoresponsive hydrogels with covalently incorporated trehalose as protein carriers. *Reactive and Functional Polymers* **2017,** *119*, 105-115.
5. Zhou, W.-J., et al., Synthesis and thermal properties of a novel lactose-containing poly(N-isopropylacrylamide-co-acrylamidolactamine) hydrogel. *Journal of Polymer Science Part A: Polymer Chemistry* **2000,** *37* (10), 1393-1402.
6. Bai, X., et al., Self-reinforcing injectable hydrogel with both high water content and mechanical strength for bone repair. *Chemical Engineering Journal* **2016,** *288*, 546-556.
7. Brannon-Peppas, L., Preparation and Characterization of Crosslinked Hydrophilic Networks. In *Studies in Polymer Science*, Brannon-Peppas, L.; Harland, R. S., Eds. Elsevier: 1990; pp 45-66.
8. Hoffman, A. S., Hydrogels for biomedical applications. *Advanced Drug Delivery Reviews* **2012,** *64*, 18-23.
9. ARES UV-curing option & photo-curing accessory. TA Instruments: 2005; Instrument Manual, pp 21-22.
10. Zuidema, J. M., et al., A protocol for rheological characterization of hydrogels for tissue engineering strategies. (1552-4981 (Electronic)).
11. Hill, A. V., The Combinations of Haemoglobin with Oxygen and with Carbon Monoxide. I. *Biochemical Journal* **1913,** *7* (5), 471-480.
12. Calvet, D., et al., Rheological Monitoring of Polyacrylamide Gelation: Importance of Cross-Link Density and Temperature. *Macromolecules* **2004,** *37* (20), 7762-7771.
13. Okay, O.; Oppermann, W., Polyacrylamide−Clay Nanocomposite Hydrogels: Rheological and Light Scattering Characterization. *Macromolecules* **2007,** *40* (9), 3378-3387.

14. Chen, T. Rheological Studies of UV - curable Materials. TA Instruments, http://www.tainstruments.com/applications-library-search/, AANO21.
15. Franck, A. Benefit of Fast Data Aquisition during Rheological Measurements. TA Instruments, http://www.tainstruments.com/applications-library-search/, APN003.
16. van Dusschoten, D.; Wilhelm, M., Increased torque transducer sensitivity via oversampling. *Rheologica Acta* **2001,** *40* (4), 395-399.
17. Du, Z., et al., Synthesis, surface and aggregation properties of glucosamide-grafted amphiphilic glycopolysiloxanes. *Colloids and Surfaces A: Physicochemical and Engineering Aspects* **2011,** *381* (1), 55-60.
18. Liang, Y.-Z., et al., Self-Association of Poly[2-(β-D-glucosyloxy)ethyl Acrylate] in Water. *Journal of Colloid and Interface Science* **2000,** *224* (1), 84-90.
19. Kulicke, W. M.; Nottelmann, H., Structure and Swelling of Some Synthetic, Semisynthetic, and Biopolymer Hydrogels. In *Polymers in Aqueous Media*, American Chemical Society: 1989; pp 15-44.
20. Nakamura, K., Interactions between Solvent Molecules and Networks in Biogels —Viscoelasticity, Strength—. In *Polymer Gels: Fundamentals and Biomedical Applications*, DeRossi, D.; Kajiwara, K.; Osada, Y.; Yamauchi, A., Eds. Springer US: Boston, MA, 1991; pp 57-75.
21. Abdurrahmanoglu, S., et al., Design of high-toughness polyacrylamide hydrogels by hydrophobic modification. *Polymer* **2009,** *50* (23), 5449-5455.
22. Ross-Murphy, S. B., Structure–property relationships in food biopolymer gels and solutions. *Journal of Rheology* **1995,** *39* (6), 1451-1463.

CHAPTER IV – Conclusions and Recommendations for Future Work

In this work, acrylamide copolymer glycohydrogels with galactose functionality were synthesized to develop a fundamental understanding of the relationship between water structuring, diffusion, and elastic properties. A range of hydrogels with varying amphipathic balance and crosslinker loading were synthesized and thoroughly examined by ^{1}H-NMR, DSC, DVS, and rheology. In collaboration with the Khare Research group at the Texas Technical University, results from experimentally measured copolymer hydrogels were used to build atomistic models of select systems which were analyzed using molecular dynamic simulations. Models complemented experimental data by providing the orientation and dynamics of water molecules around select hydrogen bonding groups. Finally, the viscoelastic properties of copolymer hydrogel systems were analyzed using an in-situ rheology technique. The main conclusions are summarized below:

1. *Water content and structural water distribution*

GalEAm copolymer hydrogels, unlike analogous DMA copolymer hydrogels, provided a range of experimentally measured high EWC systems. Tunable bound water content within GalEAm copolymer hydrogels was highest with high loading of hydrophobic monomer and crosslinker, suggesting a synergistic interplay between amphipathic balance and crosslink density on experimentally measured bound water content. Although copolymer GalEAm hydrogels possess a high propensity for water-polymer hydrogen bonding through GalEAm-OH groups, simulations showed slower mobility of water bound to hydrophilic sites in close proximity to hydrophobic groups compared to water surrounded by a hydrophilic environment. Therefore, hydrogen

bonding propensity alone cannot be used to tailor bound water content in glycohydrogels. Rather, the favorable formation of water-polymer hydrogen bonding depends both on the immediate surrounding environment of hydrogen-bonding groups along the polymer backbone.

2. *Relationship between structural water, dehydration characteristics, and water mobility*

Select GalEAm copolymer hydrogels containing high and low levels of bound water were evaluated for their desorption characteristics using DVS. The rate of desorption for GalEAm hydrogels was dependent on the relative humidity of their environment and the level of bound water, where calculated diffusion coefficients were lower for high bound water content GalEAm hydrogels. Similar trends were observed in simulations where the translational mobility of bulk water molecules decreased with increased bound water content GalEAm copolymer hydrogels containing high loading of ATris. Therefore, the concentration of bound water around hydrophilic polymer groups does impact water mobility thereby affecting desorption characteristics of hydrophobically modified glycohydrogels.

3. Rheological properties

Rheological analysis of the sol/gel kinetics and modulus as a function of frequency provided information about the hydrogel structure. Viscoelastic profiles for homopolymer GalEAm hydrogels exhibited behavior indicative of the formation of inter/intra molecular hydrogen bonded clusters between pendent saccharide moieties. The inclusion of ATris disrupted hydrogen bonding events between pendent saccharide groups in the GalEAm hydrogels, resulting in slightly longer time to gelation and drastically lower G_p'. Results

from the rheological analysis of GalEAm and DMA hydrogel architectures align well with behaviors observed from the structural water analysis in Chapter II.

4.1 Recommendations for future work

The rheological properties of the hydrogels reported in this dissertation were analyzed only as prepared using DMSO as the solvent system. It is important to note that as prepared hydrogel samples may still contain unreacted materials depending on the system. Although modulus is typically dominated by the elastic response for chemically crosslinked hydrogels, unreacted materials can affect the sample's rheological properties depending on the type of test being implemented and should be considered when using this technique. The swelling solvent will affect network dimensions (e.g., extended or collapsed morphology) and mechanical properties, therefore further evaluation of the mechanical properties for hydrogels presented in this work swollen in water would provide additional understanding of the relationship between structural water, network morphology, and modulus.

It is evident from the research reported in this dissertation that hydrophobic modification of glycopolymer hydrogels through incorporation of hydrophobic comonomers is essential to promote water-polymer hydrogen bonding and inhibit dehydration. Since limited research has been done in the area of hydrophobically modified glycopolymer hydrogels, there is a large library of potential biocompatible hydrophobic monomers that could be investigated. One area of study that may benefit from additional research in hydrophobically modified glycohydrogels is targeted drug delivery vehicles where favorable interactions between pendent saccharides and cell surface carbohydrate binding proteins can facilitate targeting capability. These systems

often require amphiphilic polymer structures in order to carry hydrophobic therapeutic loads through the body and trigger payload release at targeted locations.

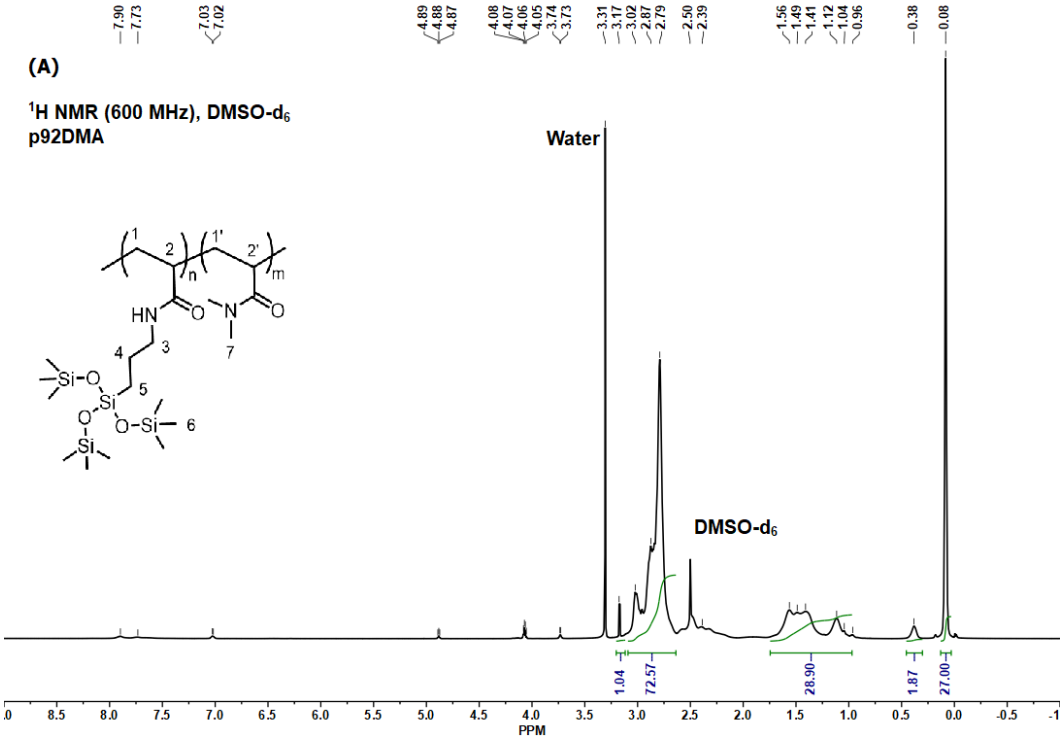
(A)
^{1}H NMR (600 MHz), DMSO-d$_6$
p92DMA
Water
DMSO-d$_6$
PPM

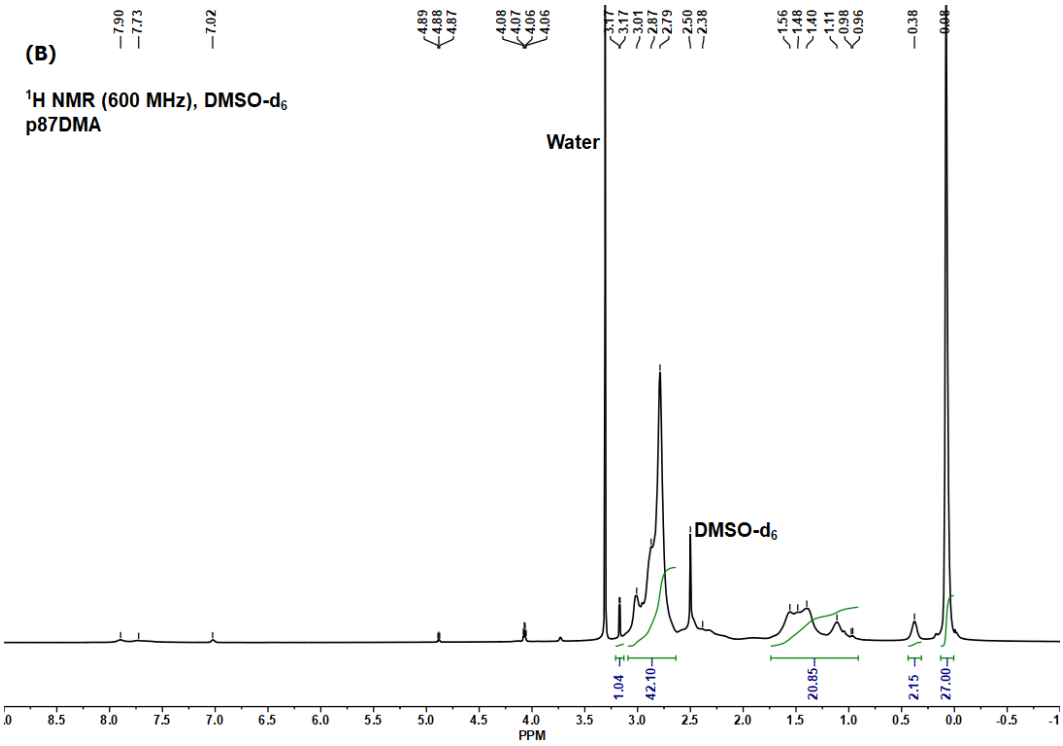
(B)
^{1}H NMR (600 MHz), DMSO-d$_6$
p87DMA
Water
DMSO-d$_6$
PPM

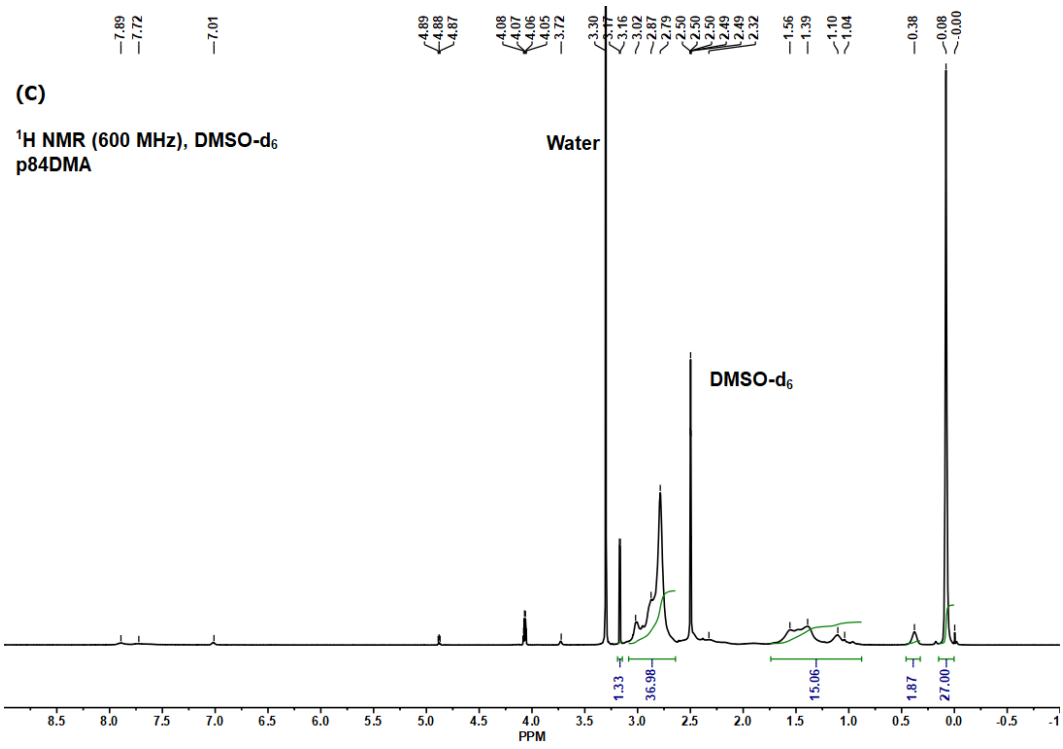

Figure A.1 ^{1}H-NMR spectra of (A) p92DMA, (B) p87DMA, and (C) p84DMA in DMSO-d6.

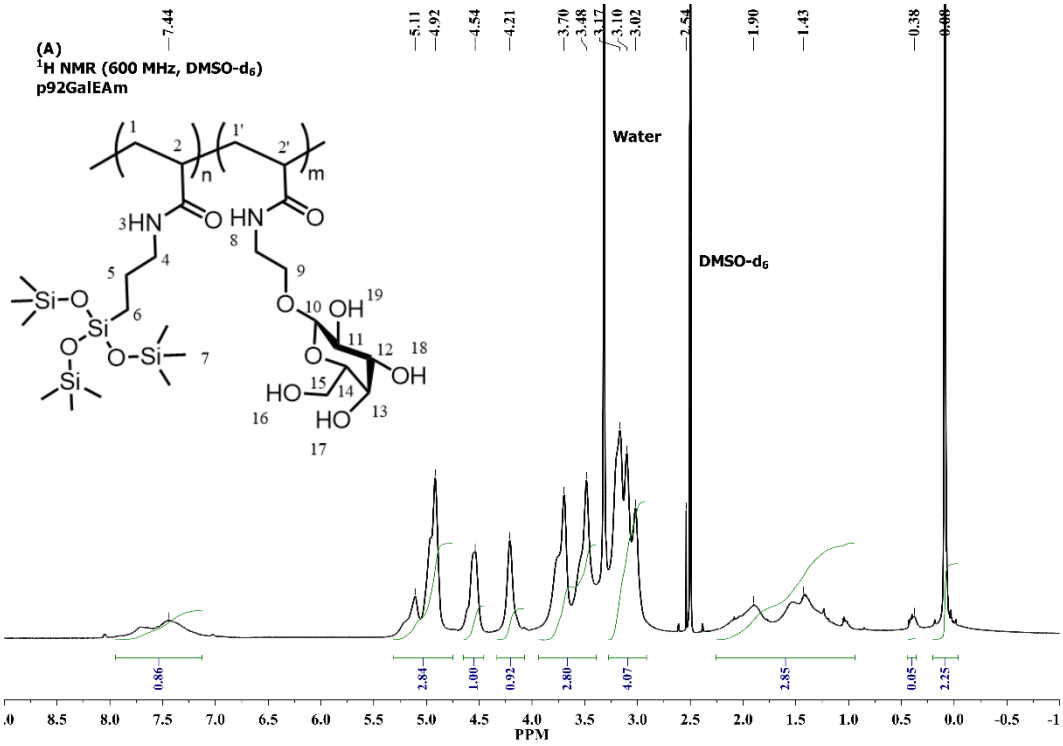

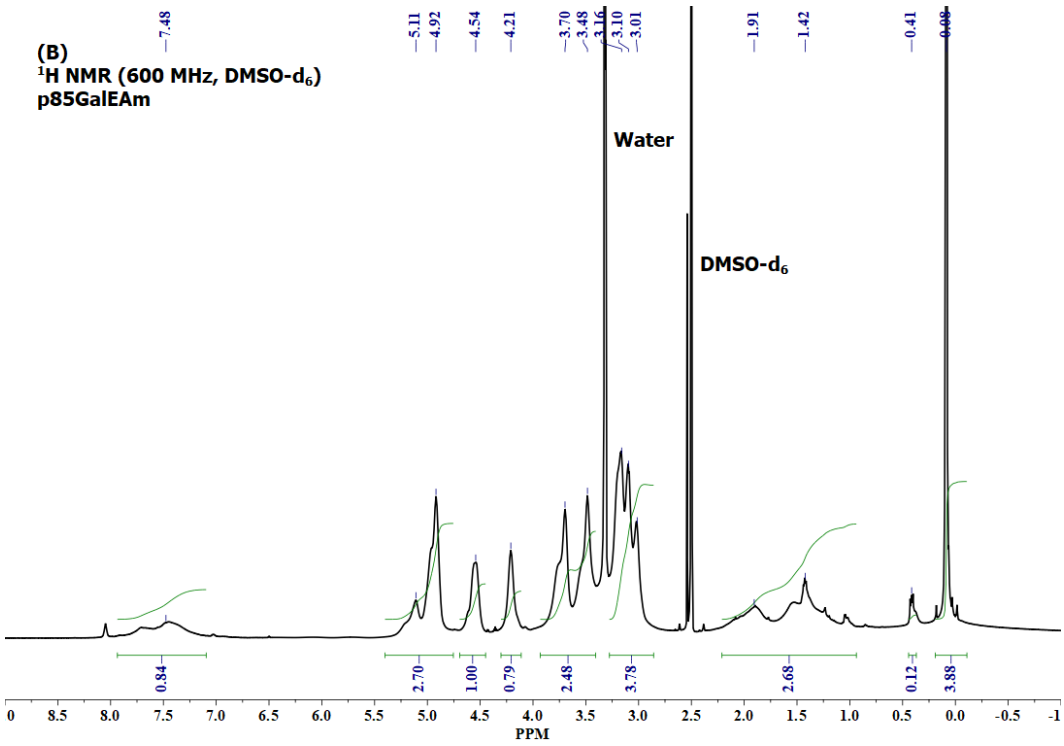

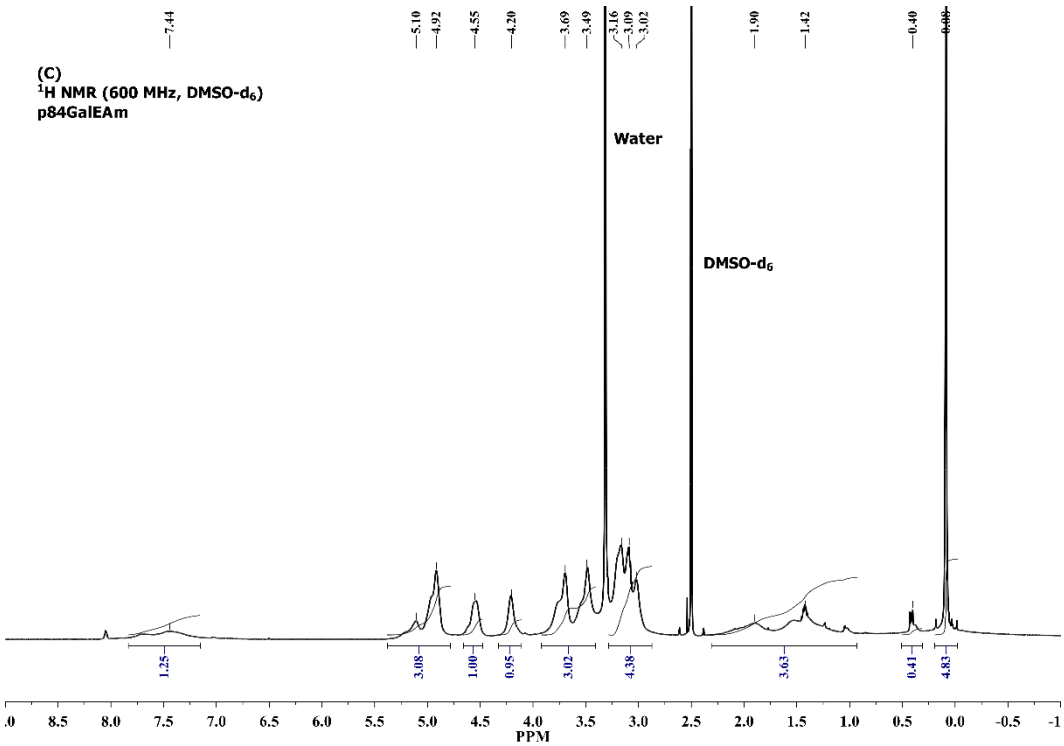

Figure A.2 ^{1}H NMR spectra of (A) p92DMA, (B) p87DMA, and (C) p84DMA in DMSO-d^6.

A.1 Force field parameters

The force field parameters, shown in Table A.1, for the silicon atom and bonded neighbor combinations in the second, third, and fourth position were taken from united atom models developed for polydimethylsiloxane (PDMS) and polyhedral oligomeric silsesquioxanes (POSS).[1-4] The united atom representations do not consider hydrogen atoms explicitly, therefore the parameters involving interactions with hydrogen atoms (e.g., O-Si-C-H in dihedrals) were taken from force-field (FF) values developed for PDMS based on quantum chemical calculations.[5]

Table A.1

Intramolecular (bonds, angles, and dihedrals) force-field parameters used in this work to describe the interactions of Si with its immediate neighbors.

Bonds: $\boldsymbol{U_b = k_b(r - r_0)^2}$		
	$k_b\left(\frac{kcal}{mol.\text{Å}^2}\right)$	$r_0(\text{Å})$
Si – O	350.12	1.64
Si – C	189.65	1.90
Angles: $\boldsymbol{U_\theta = k_\theta(\theta - \theta_0)^2}$		
	$k_\theta\left(\frac{kcal}{mol.rad^2}\right)$	$\theta_0(degree)$
Si – O – Si	14.14	146.46
Si – C – C	39.52	112.67
Si – C – H	28.77	111.09
O – Si – O	94.50	107.82
O – Si – C	49.97	110.69
C – Si – C	49.97	109.24

Dihedrals: $\boldsymbol{U_\phi = k_\phi(1 + dcos(n\phi))}$			
	$k_\phi\left(\frac{kcal}{mol}\right)$	d	n
Si – O – Si – C	0.01	1	3
O – Si – O –Si	0.225	1	1
O – Si – C – C	0.07	1	3
O – Si – C – H	0.075	1	3
C – Si – C – H	0.075	1	3

A.2 Optimization procedure for non-bonded interactions.

The non-bonded interaction parameters were calculated using the following procedure. The ε (0.11 kcal/mol) and σ (4.15 Å) values were optimized in a series of iterative simulations to reproduce the experimental density values of compounds that resemble ATris structurally and chemically (Table A.2). The initial guess values of ε and σ that were needed for this iterative procedure were taken from the Lennard-Jones (LJ)

parameters for silicon based on COMPASS FF.[6] The partial charges on the pendant group (marked by dashed red line in Figure A.3) of the ATris monomer were also determined iteratively. For this purpose, the charges associated with the entire ATris monomer was first determined using the AM1-BCC method.[7, 8] The partial charges of the pendant group were then rescaled such that the partial charge on the center silicon atom (denoted by *) was 0.75 *e* (*e* denotes the charges of an electron), which is the value determined for PDMS by quantum chemistry calculations.[5] These values were iteratively changed until the densities obtained from simulations are within 3% of the reported values of the ATris-like monomers shown in Table A.2.

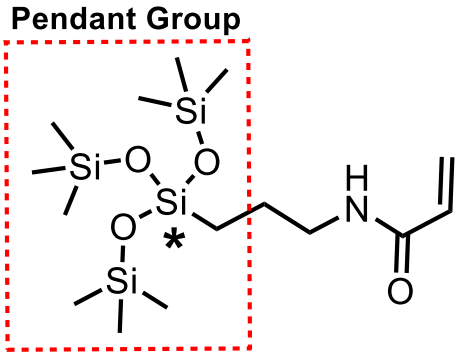

Figure A.3 Structure of ATris monomer showing the pendant groups (dashed red box) and the center silicon atom (marked with an asterisk) used to calculate non-bonded interactions.

Table A.2

Density values of ATris-like chemical compounds and their respective values obtained from simulations using the optimized non-bonded interaction parameters.

ATris-like chemical compounds	Density (g/cc)[a]	Simulation Density (g/cc)[b]
3-[Tris(trimethylsiloxy)silyl] propyl methacrylate	0.918	0.944
Tris(trimethylsiloxy) silane	0.852	0.879
3-[Tris(trimethylsiloxy)silyl] propyl vinyl carbamate	0.972	0.973

[a] Density reported in material safety data (MSDS) sheet at 25 ˚C[9-11]

[b] Generated using the optimized parameters

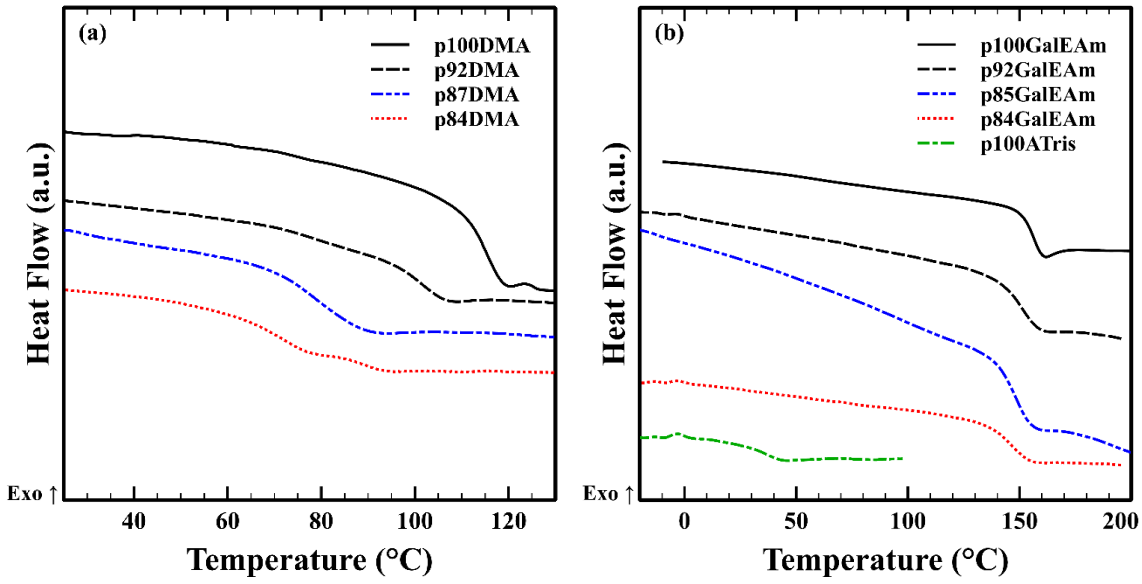

Figure A.4 Glass transition temperatures of (a) pDMA and (b) pGalEAm homo- and copolymers.

Table A.3

Analysis of variance for the effect of amphipathic ratio and crosslink density on EWC in (a) GalEAm and (b) DMA copolymer hydrogels.

(a)

Source	Adj SS	Adj MS	F-Value	P-Value
Model	1347.90	168.487	52.15	0.000
Linear	1342.41	335.603	103.87	0.000
ATris Loading	155.40	77.700	24.05	0.000
BIS Loading	1187.01	593.506	183.69	0.000
2-Way Interactions	5.49	1.372	0.42	0.789
ATris Loading*BIS Loading	5.49	1.372	0.42	0.789
Error	58.16	3.231		
Total				

(b)

Source	Adj SS	Adj MS	F-Value	P-Value
Model	340.913	42.614	35.16	0.000
Linear	285.134	71.284	58.81	0.000
ATris Loading	282.433	141.217	116.50	0.000
BIS Loading	2.701	1.351	1.11	0.350
2-Way Interactions	55.779	13.945	11.50	0.000
ATris Loading*BIS Loading	55.779	13.945	11.50	0.000
Error	21.819	1.212		
Total	362.732			

A.3 Criteria for classifying water molecule mobility

The mean-squared displacement (MSD) of water molecules in different hydration shells near the polymer groups is shown in Figure A.5. To classify water molecules based

on hydration shells, the following procedure was adopted. In the first step, the structural arrangement of water molecules around the polymer groups was determined by calculating the respective radial distribution functions (RDF). Then, the radius of the first hydration shell (r_1) for each polymer group was identified as the position of the first minimum from the respective RDF. The second and third hydration shell radius were then defined as multiples of the first hydration shell radius (i.e. $r_k^n = k \times r_1^n, k = 2,3$ and $n = -OH, -CONH$). The MSD of water molecules in each of the hydration shells was then calculated separately. For this purpose, the positions of the water molecules in different hydration shells were tracked as a function of time, starting from a reference time. Many such reference times were chosen, and the final MSD was calculated as an average over all such trajectories. The MSD of bulk water molecules is also shown in Figure A.8 for comparison. It can be seen that the water molecules near the polymer groups exhibit reduced translational mobility (as explained in the main text). A cut-off distance was defined for each polymer group based on the reduced mobility and all water molecules that lie within the specified cut-off distance was classified as bound water. The total bound water was then calculated as the sum over all the bound waters identified for each polymer group. The cut-off distance for each polymer group is as follows: GalEAm hydroxyl group – 8.0 Å, GalEAm CONH – 10.5 Å, and ATris CONH – 10.5 Å

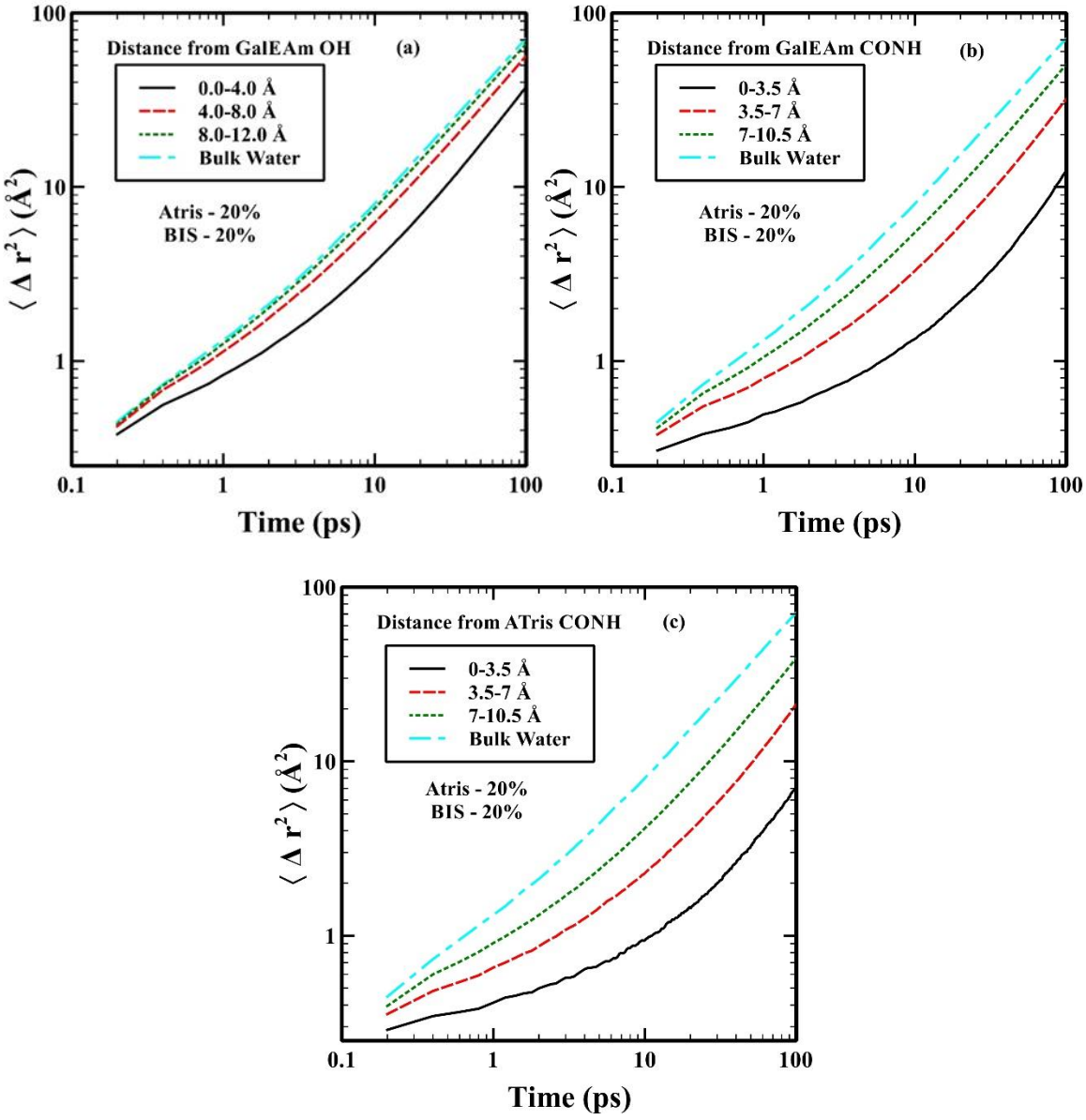

Figure A.5 Mobility of water molecules that were located in different hydration shells of (a) GalEAm hydroxyl groups, (b) GalEAm CONH groups, and (c) ATris CONH groups in GalEAm hydrogels .

Table A.4

Analysis of variance for the effect of amphipathic ratio and crosslink density on bound water in (a) GalEAm and (b) DMA copolymer hydrogels.

(a)	**Source**	**Adj SS**	**Adj MS**	**F-Value**	**P-Value**
	Model	2059.9	257.49	4.94	0.002
	Linear	572.7	143.16	2.75	0.061
	ATris Loading	192.8	96.42	1.85	0.186
	BIS Loading	379.8	189.91	3.64	0.047
	2-Way Interactions	1487.2	371.81	7.13	0.001
	ATris Loading*BIS Loading	1487.2	371.81	7.13	0.001
	Error	938.4	52.14		
	Total				
(b)	**Source**	**Adj SS**	**Adj MS**	**F-Value**	**P-Value**
	Model	1000.4	125.04	2.22	0.076
	Linear	747.6	186.90	3.32	0.033
	ATris Loading	225.8	112.89	2.00	0.164
	BIS Loading	521.8	260.91	4.63	0.024
	2-Way Interactions	252.8	63.19	1.12	0.377
	ATris Loading*BIS Loading	252.8	63.19	1.12	0.377
	Error	1014.3	56.35		
	Total	2014.6			

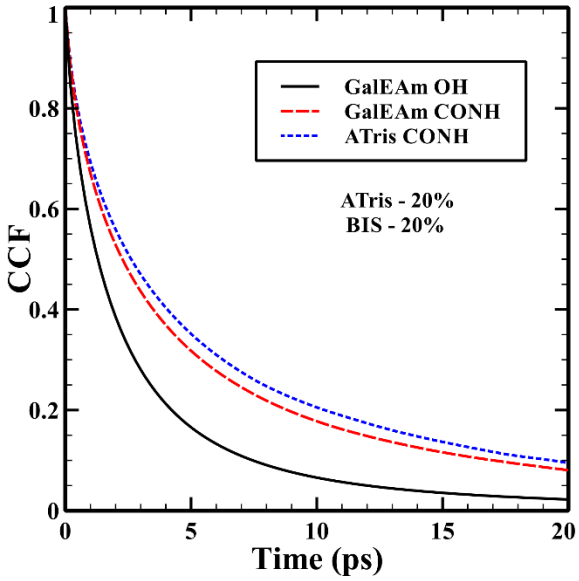

Figure A.6 Continuous correlation function (CCF) of water-water hydrogen bonds in the first hydration shell of polymer hydrogen bonding groups for GalEAm hydrogel at 20% ATris and 20% BIS loading.

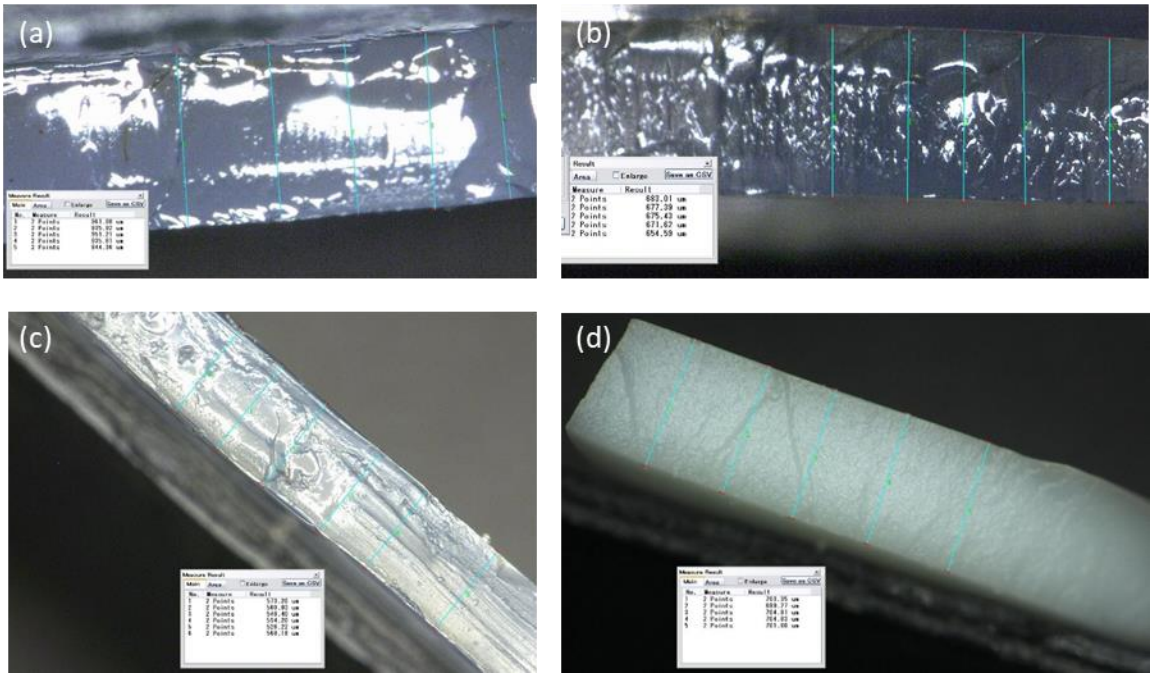

Figure A.7 Thicknesses of hydrated (a) h90GalEAm, (b) h70GalEAm, (c) h90DMA, and (d) h70DMA copolymer hydrogels with 20 mol% crosslinker selected for DVS testing.

Table A.5

Results of a two-sample t-test used to evaluate the difference between means for DMA and GalEAm hydrogels containing high and low ATris loading.

Hydrogel Means Evaluated		**35% RH**	**60% RH**	**95% RH**
h92DMA20BIS	p-Value	0.037	0.014	0.025
h92GalEAm20BIS	t-score	5.04	5.21	6.24
h84DMA20BIS	p-Value	0.962	0.294	0.002
h84GalEAm20BIS	t-score	0.05	-1.41	21.31
h92GalEAm20BIS	p-Value	0.07	0.045	0.002
h84GalEAm20BIS	t-score	2.77	3.32	-21.18
h92DMA20BIS	p-Value	0.029	0.011	0.159
h84DMA20BIS	t-score	-3.95	9.46	-2.20

[a] A zero difference between means was hypothesized where the null hypothesis is $\mu_1 - \mu_2 = 0$ and the alternative hypothesis is $\mu_1 - \mu_2 \neq 0$.

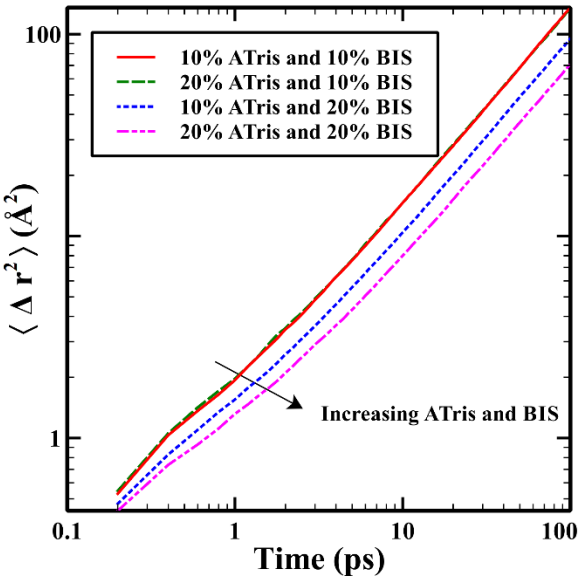

Figure A.8 Mean squared displacement of bulk water molecules in GalEAm gels at different ATris loading and cross-linker density.

A.4 References

1. Striolo, A., et al., Effective Interactions between Polyhedral Oligomeric Sislesquioxanes Dissolved in Normal Hexadecane from Molecular Simulation. *Macromolecules* **2005,** *38* (21), 8950-8959.
2. Striolo, A., et al., Thermodynamic and Transport Properties of Polyhedral Oligomeric Sislesquioxanes in Poly(dimethylsiloxane). *The Journal of Physical Chemistry B* **2005,** *109* (30), 14300-14307.
3. Habenschuss, A., et al., Structure of Poly(dialkylsiloxane) Melts: Comparisons of Wide-Angle X-ray Scattering, Molecular Dynamics Simulations, and Integral Equation Theory. *Macromolecules* **2007,** *40* (19), 7036-7043.
4. Frischknecht, A. L.; Curro, J. G., Improved United Atom Force Field for Poly(dimethylsiloxane). *Macromolecules* **2003,** *36* (6), 2122-2129.
5. Smith, J. S., et al., A Quantum Chemistry Based Force Field for Poly(dimethylsiloxane). *The Journal of Physical Chemistry B* **2004,** *108* (52), 20340-20350.
6. Sun, H.; Rigby, D., Polysiloxanes: ab initio force field and structural, conformational and thermophysical properties. *Spectrochimica Acta Part A: Molecular and Biomolecular Spectroscopy* **1997,** *53* (8), 1301-1323.
7. Araz, J., et al., Fast, efficient generation of high-quality atomic charges. AM1-BCC model: I. Method. *Journal of Computational Chemistry* **2000,** *21* (2), 132-146.
8. Araz, J., et al., Fast, efficient generation of high-quality atomic charges. AM1-BCC model: II. Parameterization and validation. *Journal of Computational Chemistry* **2002,** *23* (16), 1623-1641.

9. Ross-Murphy, S. B., Structure–property relationships in food biopolymer gels and solutions. *Journal of Rheology* **1995,** *39* (6), 1451-1463.
10. 3-[Tris(trimethylsiloxy)silyl] propyl methacrylate MSDS no: 446130. Aldrich, S., Ed. 2016.
11. 3-[Tris(trimethylsiloxy)silyl] propyl vinyl carbamate MSDS no: 795402. Aldrich, S., Ed. 2016.

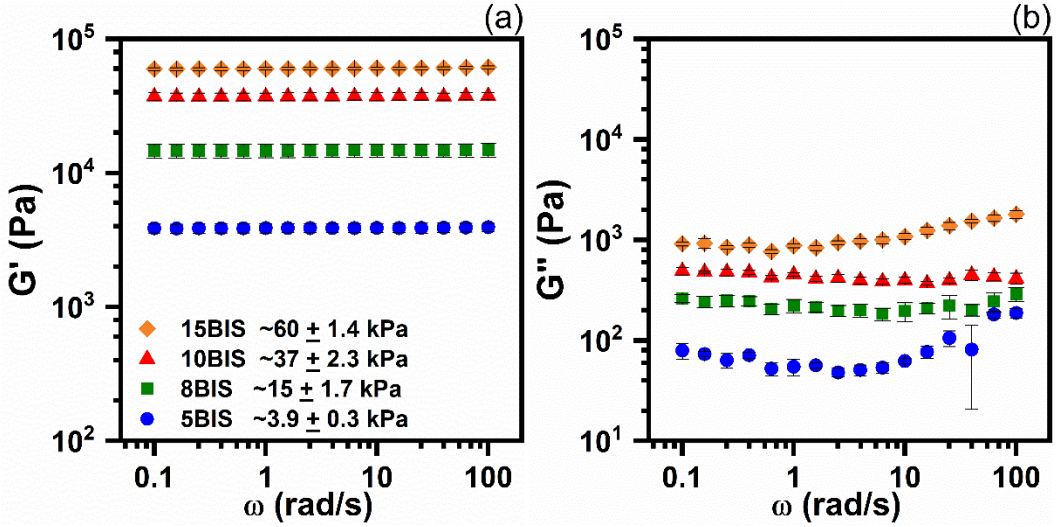

Figure B.1 The average storage (a,c) and loss (b,d) modulus of h100GalEAm (top) and h100DMA (bottom) with varying BIS loading as a function of frequency (ω) ramped from 100 to 0.1 rad/s. The calculated average ± standard deviation is embedded in the G' figure legend.

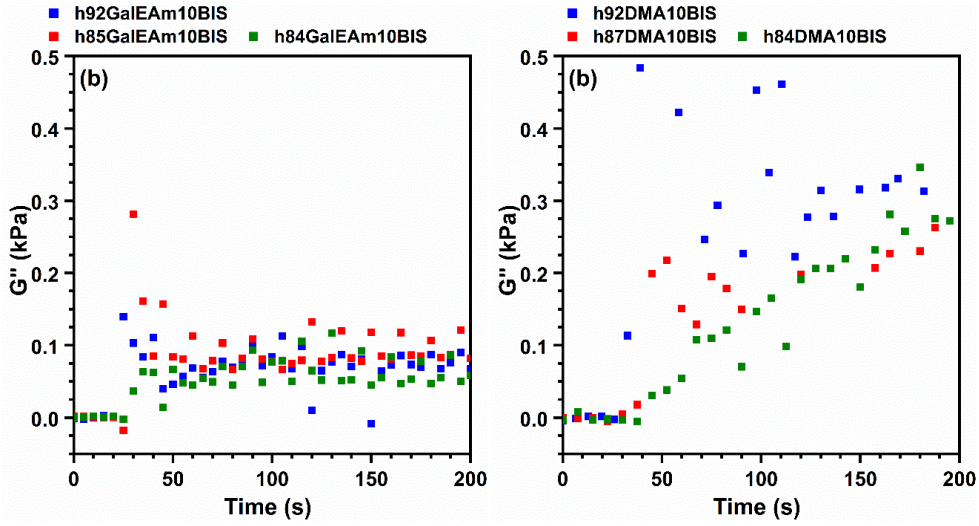

Figure B.2 The magnitude of G" from rheokinetic measurements of (a) hGalEAm10BIS and (b) hDMA10BIS with varying ATris loading is negligible, indicating that the hydrogel modulus is dominated by elastically effective crosslinked nature.